TAMPERE UNIVERSITY OF TECHNOLOGY

MIMMI VIHERKOSKI

SIGMA-PHASE FORMATION IN HEAT-RESISTANT CAST STAINLESS STEELS

Master of Science Thesis

Examiner: Professor Tuomo Tiainen
Examiner and topic approved in the Faculty of Automation, Mechanical and Materials Engineering Council Meeting on February 8th 2012

ABSTRACT

TAMPERE UNIVERSITY OF TECHNOLOGY
Master's Degree Programme in Materials Science
VIHERKOSKI, MIMMI: Sigma-Phase Formation in Heat-Resistant Cast Stainless Steels
Master of Science Thesis, 66 pages
April 2012
Major: Metallic Materials
Examiner: Professor Tuomo Tiainen
Keywords: cast stainless steels, sigma-phase, embrittlement, impact toughness

Heat-resistant cast stainless steels are widely favoured materials for their resistance to corrosion even at elevated temperatures. These steels maintain their good mechanical properties, for example high strength, even when the material is heated above 650 °C. However, when they are cooled to room temperature, embrittlement often takes place. This loss in ductility is usually due to the formation of the sigma-phase, which is hard and extremely brittle.

This thesis focuses on the formation of the sigma-phase. The factors that affect the formation are presented and studied individually. The theoretical part includes also background information of cast stainless steels and heat-resistant steel grades. The embrittlement phenomenon is discussed in more detail. Probable causes for embrittlement are briefly discussed one by one. The emphasis is kept on the sigma-phase. The question of how the sigma-phase influences the mechanical properties of the steel is covered as well.

The experimental part consisted of the studies on the influences of the sigma-phase on the mechanical properties. The test series was started with long-term exposure (aging) at elevated temperature. Impact toughness tests were performed in order to find out the possible connection between the aging time and the eventual changes in ductility. In addition, hardness values were measured. The experimental part included also microstructural characterisation. Optical microscopy was used in the microstructural characterisation of all test samples. Part of the test samples was characterised using scanning electron microscopy (SEM) and energy dispersive spectroscopy (EDS).

The studied samples showed a major decrease in the impact toughness with increasing time of aging, whereas the hardness values showed only a slight increase. Microstructural characterisation revealed significant changes in the microstructures of the samples between different steel grades and different times of aging.

TIIVISTELMÄ

TAMPEREEN TEKNILLINEN YLIOPISTO
Materiaalitekniikan koulutusohjelma
VIHERKOSKI, MIMMI: Sigma-faasin muodostuminen tulenkestävissä ruostumattomissa valuteräksissä
Diplomityö, 66 sivua
Huhtikuu 2012
Pääaine: Metallimateriaalit
Tarkastaja: professori Tuomo Tiainen
Avainsanat: ruostumattomat valuteräkset, sigma-faasi, haurastuminen, iskusitkeys

Ruostumattomat teräkset kestävät hyvin korroosiota korkean kromipitoisuutensa vuoksi. Muokkaaminen ja valaminen ovat tavallisia terästen ja terästuotteiden valmistusmenetelmiä. Valamista suositaan esimerkiksi edullisempien tuotantokustannusten takia. Lisäksi valamalla on mahdollista valmistaa suuria ja monimutkaisia yksityiskohtia sisältäviä kappaleita, mikä ei ole mahdollista muokkaavia työstömenetelmiä käyttämällä.

Tulenkestävät ruostumattomat valuteräkset ovat korroosionkestäviä myös korkeissa lämpötiloissa. Tästä syystä niitä käytetään useissa sovelluksissa. Lisäksi nämä teräkset säilyttävät hyvät mekaaniset ominaisuutensa, kuten korkean lujuuden, jopa yli 650 °C lämpötiloissa. Nämä materiaalit voivat kuitenkin olla hieman ongelmallisia, siksi että ne monesti menettävät sitkeysominaisuutensa jäähdytettäessä huoneenlämpötilaan. Useasti haurastuminen johtuu kovan ja erittäin hauraan sigma-faasin muodostumisesta.

Tässä diplomityössä keskitytään sigma-faasin muodostumiseen tulenkestävissä ruostumattomissa valuteräksissä. Muodostumiseen vaikuttavat useat eri tekijät kuten aika, lämpötila sekä materiaalin mikrorakenne ja koostumus. Jokainen tekijä käsitellään teoriaosassa yksitellen. Teoriaosassa tutustutaan myös yleisesti ruostumattomiin valuteräksiin ja tulenkestävien terästen ominaisuuksiin. Haurastumisilmiöitä käsitellään laajemmin. Mahdolliset haurastumiseen vaikuttavat tekijät esitellään yksitellen, kuitenkin koko ajan sigma-faasiin keskittyen. Myös sigma-faasin vaikutukset materiaalin mekaanisiin ominaisuuksiin ovat tärkeä osa teoreettista tarkastelua.

Kokeellinen osa koostui mekaanisten ominaisuuksien mittauksista sekä mikrorakennetarkasteluista. Itse testaus aloitettiin testikappaleiden pitkäaikaisella lämpötila-altistuksella (vanhennus) korkeassa lämpötilassa. Iskusitkeyskokeiden tarkoituksena oli selvittää mahdollinen yhteys eri vanhennusaikojen ja materiaalien haurastumisen välillä. Lisäksi testikappaleiden kovuudet mitattiin. Kaikki testikappaleet tutkittiin optisella mikroskoopilla. Pyyhkäisyelektronimikroskopiaa ja alkuaineanalysaattoria käytettiin karakterisoitaessa osaa näytteistä.

Tutkimuksessa saadut tulokset tukevat aiempia tutkimustuloksia. Tutkittujen materiaalien iskusitkeydet laskevat merkittävästi vanhennusaikojen kasvaessa. Toisaalta taas kovuusarvoissa oli havaittavissa ainoastaan pientä kasvua. Mikrorakennetarkastelut paljastivat huomattavia muutoksia mikrorakenteissa eri teräslajien ja vanhennusaikojen välillä.

ACKNOWLEDGEMENTS

This Master's Thesis was carried out in the Department of Materials Science in Tampere University of Technology during September 2011 - April 2012 as a part of a bigger FIMECC project DEMAPP Melt. Metso Minerals Oy was the co-operating company in the project. I am grateful for all the help I was given during this thesis and my studies.

First of all my thanks go to Professor Tuomo Tiainen. His guidance has been a great support. I also thank him for examining this thesis. Mikko Uusitalo and Tuomas Himanka from Metso Minerals Oy have offered me their expertise and good advice. I am grateful for the opportunity to study this interesting field of steel materials.

The Department of Materials Science and its personnel have my gratitude for all their help and guidance with the machining and laboratory measurements.

Special thanks go to my friends and my family. I acknowledge my fellow students and especially my closest friends for their understanding and support during my studies and particularly during this thesis. Matti has been my rock and my dearest thanks go to him for his priceless support. Finally, I want to thank my family; my mother for her endless confidence in my abilities, and my late father for opening my eyes to the world of science.

Tampere, Finland
April 19th 2012

Mimmi Viherkoski

CONTENTS

ABBREVATIONS AND NOTATION

αFe	α-Ferrite
at%	Atomic percent
bcc	Body-centered cubic
BSE	Backscattered electron
C-type	Corrosion-resistant cast stainless steel
Cr_e	Chromium equivalent
δFe	δ-Ferrite
d_1	Diameter of the trace
DEMAPP	Demanding Applications; a group of FIMECC projects
EDS	Energy dispersive spectroscopy
fcc	Face-centered cubic
γFe	Austenite
h	Hour
H-type	Heat-resistant cast stainless steel
HRC	Rockwell C scale hardness
HV	Vickers hardness number
J	Joule
mm^2	Square millimetre
N	Newton
$\bar{N}_v$	Electron hole number
Ni_e	Nickel equivalent
P	Applied load
SE	Secondary electron
SEM	Scanning electron microscopy
σ	Sigma-phase
vol%	Volume percent
wt%	Weight percent
χ	Chi-phase

Al	Aluminium
C	Carbon
Co	Cobalt
Cr	Chromium
Cr_7C_3	Chromium carbide
$Cr_{23}C_6$	Chromium carbide
Cu	Copper
Fe	Iron
HNO_3	Nitric acid
Ma	Manganese
Mo	Molybdenum

N	Nitrogen
NaOH	Sodium hydroxide
Nb	Niobium
Ni	Nickel
P	Phosphor
S	Sulphur
Si	Silicon
Ti	Titanium
V	Vanadium
W	Tungsten

1 INTRODUCTION

Stainless steels are divided into two categories: cast stainless steels and wrought stainless steels. Casting can be chosen as a shaping method for stainless steel products for a variety of reasons. Cast products require little or no machining. Casting enables the production of highly complex and large shapes. Almost any type of material can be cast, even the most brittle ones.

Cast stainless steels are designed for either high temperature (heat-resistant) or corrosive (corrosion-resistant) operating conditions. These heat-resistant and corrosion-resistant cast stainless steels are categorised into different grades depending on their microstructure and composition. In this study the focus is on the heat-resistant cast steels with austenitic or ferritic-austenitic microstructures.

Heat-resistant cast steels are designed for the use at temperatures above 650 °C. These steels differ from corrosion-resistant cast steels by their lower ductility, poorer corrosion-resistance, and greater strength at elevated temperatures. In practice this difference in their strength results from the higher carbon content of the heat-resistant alloys, generally ranging up to the maximum of 0.75 wt%. The main concern with heat-resistant cast steels is the changes in the properties which may take place when the material is cooled to lower temperatures from its operating temperature. Usually the embrittlement of the material is the most detrimental change.

The embrittlement of the material can originate from a variety of reasons. Higher carbon content of the alloy in chromium-rich stainless steels can lead to the precipitation of different types of carbides. The ductility is affected less if the carbides are finely dispersed throughout the microstructure. The ductility is strongly reduced if the carbides form continuous networks in the microstructure, for example on grain boundaries. The root of the embrittlement still often lies in the formation of the sigma-phase. This phase is a hard and extremely brittle intermetallic phase that forms within the temperature range of 650-870 °C. It does not necessarily influence the ductility at elevated temperatures. Its embrittling effect is most detrimental when the material is cooled to the room temperature. In practice this occurs, for example, when an engine component made of heat-resistant cast steel is cooled for maintenance or repair.

Several factors influence the formation of the sigma-phase. The key is to learn how these factors could be controlled to minimise or prevent its formation. If the steel composition and the operating conditions do not allow these adjustments and the sigma-phase is formed, then it is important to know the influences it has on the properties of the material.

2 CAST STAINLESS STEELS

Stainless steels differ from other steels especially by their resistance to corrosion and oxidation. The alloying with more than 10 wt% chromium enables the use of these steels in aqueous environments. Cast stainless steels are divided into two major groups; corrosion-resistant (C-type) and heat-resistant (H-type). Corrosion-resistant castings are mainly designed for the use at temperatures below 650 °C, whereas heat-resistant ones are suitable for operating temperatures above 650 °C. This division, however, is not always definite and therefore the carbon content is mostly used as a divider between these two cast steel types. Heat-resistant grades have higher carbon contents. [1]

Cast stainless steels are designated according to the standard ASTM A781/A 781M (Appendix X1) [2]. The designation is rather straightforward. As previously stated, the first letter of the designation denotes whether the alloy is of corrosion-resistant (C) or heat-resistant (H) type. The following letter refers to nickel and chromium contents of the alloy. These contents and their equivalent letters are shown in Figure 2.1 [1].

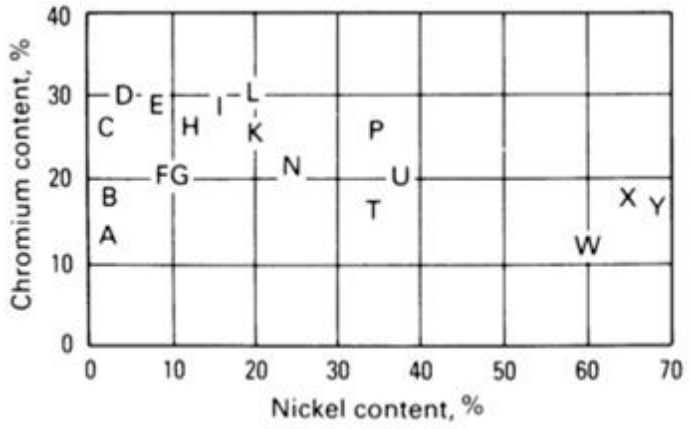

Figure 2.1. *Nickel and chromium contents of cast stainless steels and their corresponding designation letters for heat- and corrosion-resistant cast steel grades. [1]*

2.1 Cast stainless steels as compared to wrought stainless steels

Though cast stainless steels can be alloyed almost similarly as wrought stainless steels, there are usually some differences. These differences lead to different microstructures and again to different properties and applications.

2.1.1 Microstructure and composition

The main factor which determines the microstructure of a particular cast steel grade is its composition. The eventual heat treatment plays also an important role. Different microstructures are austenitic, ferritic, ferritic-austenitic (duplex), and martensitic. Chromium, molybdenum, silicon, and niobium are ferrite promoters. The alloying elements which promote austenite formation are nickel, carbon, nitrogen, and manganese. The chromium and nickel contents mainly determine the microstructure of an iron-based alloy. [3]

Cast austenitic stainless steels differ from wrought austenitic stainless steels in terms of their ferrite content. Wrought austenitic grades are alloyed to be fully austenitic in order to achieve reduced strength and some ductility to ease rolling and forging [4]. Cast austenitic grades, on the other hand, usually have some ferrite distributed in the matrix. Ferrite is utilized to improve weldability and corrosion resistance. The resistance to stress-corrosion cracking also increases with increasing ferrite content. However, the influence of ferrite can also be detrimental, especially in elevated temperature applications since ferrite is susceptible to embrittlement when exposed to temperatures of 315 °C and higher. [3]

As mentioned earlier, wrought stainless steels need to have a fully austenitic microstructure due to the way they are formed. Cast stainless steels can be produced with compositions which are not feasible for wrought stainless steels. Therefore cast alloys may possess superior mechanical and physical properties as compared to wrought alloys. [4] In general cast alloys have higher chromium and silicon contents to promote the formation of ferrite. On the other hand their nickel contents are usually lower than in wrought alloys.

2.1.2 General properties

Cast stainless steels have many advantages as compared to wrought stainless steels. The following properties apply to all cast alloys. Typically they are lower in price since they require less machining. In most cases the cast part is complete directly after casting. Casting can also produce a variety of highly complex and large shapes which cannot be fabricated otherwise. [5]

Low ductility alloys can be impossible to form by hot or cold working. This is a problem especially with high chromium alloys. However, such alloys can be cast. Their brittleness, on the other hand, has to be taken into consideration. Once a brittle material is cast and it is in service, it can lose more of its ductility. This could lead to further problems in, for example, welding and room temperature properties. [6]

One advantage in cast stainless steels is their creep strength. Cast components are basically stronger at high temperatures than wrought ones. This is due to the microstructure and higher carbon content of cast steels. [6]

2.2 Heat-resistant cast steels

According to Metals Handbook ”Castings are classified as heat resistant if they are capable of sustained operation while exposed, either continuously or intermittently, to operating temperatures that result in metal temperatures in excess of 650 °C.” Heat-resistant steels can be divided into three categories depending on their composition: iron-chromium, iron-chromium-nickel, and iron-nickel-chromium. They all possess resistance to corrosion at elevated temperatures, stability, and good creep strength values. [3]

2.2.1 Microstructure

The microstructures of heat-resistant cast steels should be completely austenitic or mainly austenitic along with some ferritic phase. As in cast stainless steels altogether, the feasible microstructures in heat-resistant grades are austenitic, ferritic, and ferritic-austenitic. In order to obtain higher strength at elevated temperatures, the austenitic phase is favoured because the ferritic phase is then rather soft and weak. This results from deformation mechanisms. At high temperatures, diffusion becomes an important deformation mechanism and the diffusion in close-packed fcc austenite is slower than in non-close-packed bcc ferrite. In addition to high strength, resistance to corrosion is valued and therefore the ferrite is not totally excluded. The formation of a certain microstructure in heat-resistant cast steel can be controlled by the selection of the composition of the raw material and alloying elements, as well as by the eventual heat treatment.

Usually cast austenitic stainless steels contain from 5 to 20 % of ferrite [1]. As stated previously, the ferrite content of the alloy can be controlled. This is done mainly by adjusting the composition. Schaeffler diagram in Figure 2.2 was first developed to give information on the welding properties. The diagram is also a useful tool for estimating the microstructure of a stainless steel. It shows different microstructures as a function of the chromium and nickel equivalents. These equivalents can be derived from the following equations (1) and (2) [7].

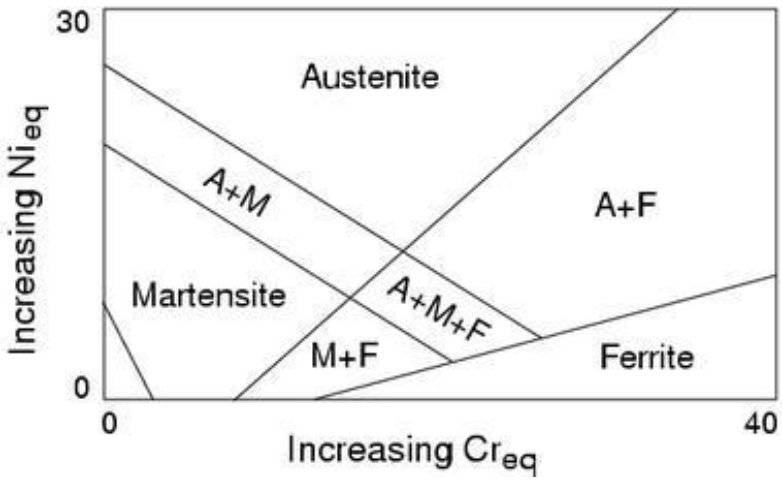

Figure 2.2. *The Schaeffler diagram. [7]*

The chromium equivalent represents the total ferritizing power of ferrite promoting elements. Respectively the total austenitizing power of austenite promoting elements is derived from the nickel equivalent. As the chromium equivalent increases, the ferrite content increases as well. Same applies to the nickel equivalent and the austenite content.

$$Cr_e = (Cr) + 2(Si) + 1.5(Mo) + 5(V) + 5.5(Al) + 1.75(Nb) + 1.5(Ti) + 0.75(W) \quad (1)$$

$$Ni_e = (Ni) + (Co) + 0.5(Mn) + 0.3(Cu) + 25(N) + 30(C) \quad (2)$$

In equations (1) and (2) the elemental contents are given in weight percents. [7]

In addition to Schaeffler diagram, Schoefer diagram is also used in estimating microstructures. Schoefer diagram in Figure 2.3 is an advanced version of the Schaeffler diagram and it is mainly used in predicting and controlling the ferrite content of an alloy. The diagram is a suitable tool for steel castings in the composition range of 16-26 % chromium, 6-14 % nickel, and maximum of 4 % molybdenum, 1 % niobium, 0.2 % carbon, 0.19 % nitrogen, 2 % manganese, and 2 % silicon. Calculating the chromium and nickel equivalents for Schoefer diagram differs slightly from the corresponding calculations for Schaeffler diagram. For Schoefer diagram, the following equations (3) and (4) are adequate. [1]

$$Cr_e = (Cr) + 1.5(Si) + 1.4(Mo) + (Nb) - 4.99 \quad (3)$$

$$Ni_e = (Ni) + 30(C) + 0.5(Mn) + 26(N - 0.02) + 2.77 \quad (4)$$

In equations (3) and (4) the elemental contents are given in weight percents. As the previous equations (1-4) show, there are many ways in calculating the chromium and nickel equivalents. The key here is to use the calculations specified for the diagram which is used.

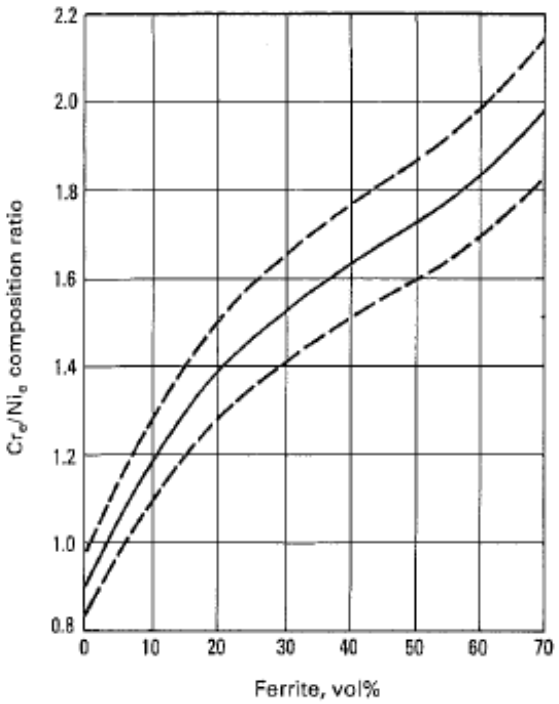

Figure 2.3. *The Schoefer diagram. [1]*

In Figure 2.3 the solid line of the Schoefer diagram denotes the ferrite content as a function of the ratio of chromium and nickel equivalents. Since the chemical analysis of different elements influencing the equivalents can be somewhat uncertain, there are dashed lines on both sides of the solid line. Considering the uncertainty of the analysis, the actual results can be found within these dashed lines. [1]

The estimation and controlling of the ferrite content is fairly simple when either Schaeffler or Schoefer diagram is used. However, there are some limitations which influence the accuracy of these estimations. First of all, the chemical analysis of an alloy is not completely accurate. This has an effect on the chromium and nickel equivalents. Also prior thermal treatments influence the ferrite content. And finally, the ferrite content depends on the casting itself. There can be much variation in the ferrite content depending on the location of the sample taken for the analysis. Section size, ferrite orientation, and segregation of the alloying elements have an effect as well. [1]

As mentioned before there are three compositional categories of heat-resistant cast steels: iron-chromium, iron-chromium-nickel, and iron-nickel-chromium. The division between each category is made depending on the composition and the consequent microstructure. The iron-chromium alloys have low strength at elevated temperatures. They contain 10-30 % chromium and have mainly ferritic microstructure. Due to their chromium content, the resistance to oxidation is good. Figure 2.4 shows the Cr-Fe phase diagram that applies to iron-chromium alloys. Alloys containing over 13.4 wt% chromium are mostly ferritic (αFe, δFe) at all operating temperatures. Austenite (γFe) is only formed when the chromium content is lower than 13.4 wt%. [1]

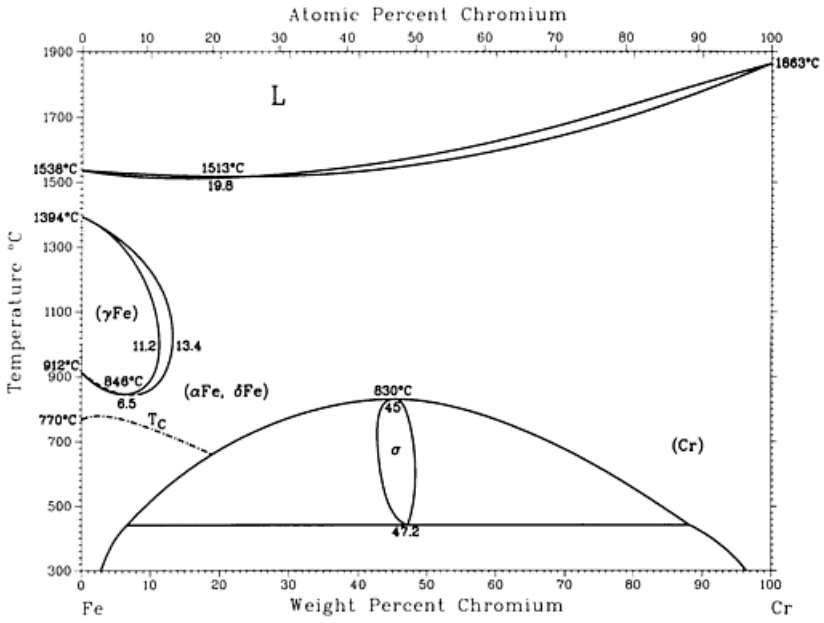

Figure 2.4. *The phase diagram of the chromium-iron alloy system. [8]*

The iron-chromium-nickel alloys exceed the iron-chromium alloys in strength and ductility. Their microstructure is mainly austenitic when containing more than 13 wt% chromium and 7 wt% nickel. The isothermal section of the ternary phase diagram of the Cr-Fe-Ni alloy system at 800 °C is shown in Figure 2.5. [1,9]

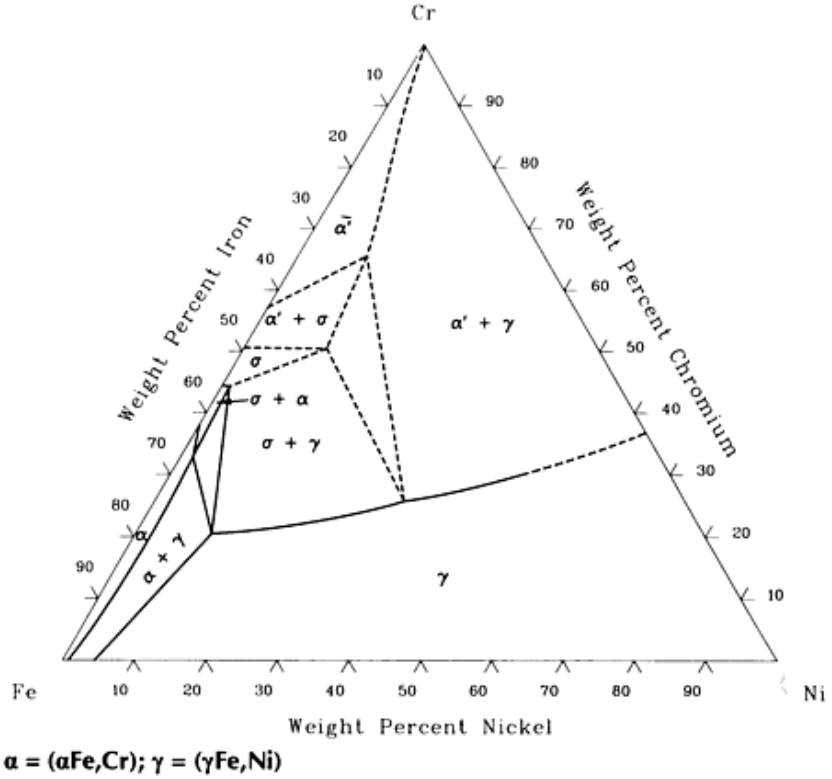

Figure 2.5. *The isothermal section of the chromium-iron-nickel alloy phase diagram at 800 °C. [9]*

The iron-nickel-chromium alloys have nickel as their major alloying element (contents exceeding 25 wt%). More than 10 wt% of chromium is added to enhance the cor-

rosion resistance. The microstructure is completely austenitic when the chromium content does not exceed approximately 23 wt% (see Figure 2.5). [1,9]

In addition to the austenite and ferrite phases, several other phases can also exist. Table 2.1 presents the secondary phases in alloyed stainless steels [10]. The precipitation of different types of carbides is common. The carbon content of the alloy is the determining factor in the carbide formation. The cooling rate of the casting during solidification is also considered as important. The chromium-rich carbide $M_{23}C_6$ is the most common carbide type. The letter M stands for the total sum of metallic elements, which participate in carbide formation. The chromium carbide M_7C_3 precipitates in higher temperature range than $M_{23}C_6$ and is therefore more uncommon. [4]

Table 2.1. *The secondary phases in alloyed stainless steels. Letter M on the Type column stands for the total sum of metallic elements. [10]*

Stainless steels(a)	Phase	Symbol	Type	Formula	Temperature range(b) °C	Temperature range(b) °F
D	Chromium carbide	. . .	M_7C_3	$(Cr,Fe,Mo)_7C_3$	950–1050	1740–1920
A,D,F	Chromium carbide	. . .	$M_{23}C_6$	$(Cr,Fe,Mo)_{23}C_6$	600–950	1110–1740
A,D,F	Chromium carbide	. . .	M_6C	$(Cr,Fe,MoNb)_6C$	700–950	1290–1740
D,F	Chromium nitride	. . .	M_2N	$(Cr,Fe)_2N$	650–950	1200–1740
D	Chromium nitride	. . .	MN	CrN	. . .	. . .
D	Fe-Mo nitride	. . .	M_5N	$Fe_7Mo_{13}N_4$	550–600	1020–1110
A	Nb-Cr nitride	Z	MN	(NbCr)N	700–1000	1290–1830
F	Titanium carbonitride	. . .	MC	Ti(CN)	700 m.p.	1290 m.p.
F	Niobium carbonitride	. . .	MC	Nb(CN)	700 m.p.	1290 m.p.
A,D,F	Sigma	σ	AB	(Fe,Cr,Mo,Ni)	550–1050	1020–1920
A,D,F	Chi	χ	$A_{48}B_{10}$	$Fe_{36}Cr_{12}Mo_{10}$ $(FeNi)_{36}Cr_{18}(TiMo)_4$	600–900	1110–1650
D,F	Alpha prime	α′	. . .	CrFe(Cr 61–83%)	350–550	660–1020
A,D,F	Laves	η	A_2B	$(FeCr)_2(Mo,Nb,Ti,Si)$	550–900	1020–1650
D,F	R	R	. . .	(Fe,Mo,Cr,Ni)	550–650	1020–1200
D	Tau	τ	. . .	. . .	550–650	1020–1200

R, R intermetallic phase. (a) Type code: A = austenitic, D = duplex, F = ferritic. (b) m.p., melting point.

The sigma (σ) -phase is an intermetallic phase, which forms in heat-resistant cast stainless steels. Sigma-phase forms readily in prolonged heating between temperatures 650-870 °C. This temperature range is highly dependent on the alloying. The ductility of this phase is poor and the occurrence of sigma-phase in a cast alloy leads to the brittleness of the material. The sigma-phase is studied in more detail in Chapter 3.1. The chi (χ) phase coexists with sigma. Chi is a hard and brittle phase, which requires molybdenum alloying for its formation. [4]

2.2.2 Alloying elements

The main alloying elements in heat-resistant stainless steels are chromium (Cr) and nickel (Ni). Chromium is used to enhance the resistance to corrosion and oxidation. [3] Chromium forms a thin protective oxide layer, a passive film that protects the metal underneath [5]. For the passive film to form, the chromium content should exceed 11 wt% [11]. Nickel on the other hand does not participate in the formation of the passivating layer but it has other advantageous effects concerning the corrosion resistance. Stainless steels alloyed with nickel have high toughness and ductility values even at

extremely low temperatures. The strengthening effect of nickel is not as good as that of chromium. [11]

There is some carbon (C) in every heat-resistant cast steel grade. Generally the maximum carbon content is 0.50 wt% [4]. Carbon promotes the formation of austenite and it is known to increase the strength of the steel. Carbon has a tendency to form precipitates with chromium. These carbides are extremely hard and therefore useful for wear resistance, but they may also lead to the deterioration of corrosion resistance because chromium migrates from solid solution to carbide particles. [11]

Other alloying elements, which are added to heat-resistant steels are manganese (Mn), silicon (Si), molybdenum (Mo), nitrogen (N), copper (Cu), and aluminium (Al). In addition, sulphur (S), and phosphor (P) exist in these structures as impurities. Some of the most significant alloying elements are discussed in the following text. Manganese can be used partly instead of nickel as an austenite promoter. It is not as expensive as nickel and therefore its use is reasonable. [12] Molybdenum is used to improve mechanical properties at elevated temperatures since it has a high melting point at 2 610 °C [11]. Molybdenum is also used in cast stainless steels to improve the general corrosion resistance. Nitrogen is present in both austenitic and ferritic phases as an interstitial element. It is added to composition mainly for solid-solution strengthening. In addition it has favourable influences on corrosion resistance. [4]

2.2.3 Heat-resistant steel grades

Heat-resistant steels are classified into different grades according to their chromium and nickel contents (see Figure 2.1 on page 2). Grades HA, HC, and HD belong to the iron-chromium alloys. Their microstructure is essentially ferritic, excluding HD, which has a two-phase ferritic-austenitic structure. Grade HA has low strength and it is susceptible to gaseous corrosion at elevated temperatures. Its chromium content is high enough for good resistance to oxidation. Grades HC and HD possess rather similar properties, except that grade HD has higher strength due to its higher nickel content. The drawback is that these grades are prone to sigma-phase embrittlement at temperatures between 650-870 °C. [13]

Iron-chromium-nickel alloys include grades HE, HF, HH, HI, HK, and HL. They all have chromium contents, which exceed their nickel contents. These alloys are primarily austenitic and therefore they exceed the iron-chromium alloys in mechanical properties, including strength and ductility. Due to its higher chromium content, grade HE has good resistance to corrosion at high temperatures, ranging up to 1100 °C. Long exposure to temperatures close to 815 °C makes grade HE brittle due to the formation of sigma-phase. Grade HF has lower chromium content than HE and therefore it is used at operating temperatures below 870 °C. It is susceptible to sigma-phase formation within temperatures 760-815 °C. Grade HH is divided into two grades depending on their structures: type I is partially ferritic and type II completely austenitic. Type I lags behind type II in creep strength and ductility. In addition type I has a greater tendency for sigma-phase formation within the temperature range of 650-870 °C. Grades HI and HK

can both be used at high temperatures reaching up to almost 1200 °C. The microstructure of grade HI is essentially austenitic. Grade HK has an austenitic structure as well. Unbalanced compositions in grade HK can result in the formation of microstructure that is mainly austenitic with some ferrite in it. The austenite can transform directly to sigma-phase between temperatures 760-870 °C [3]. For the ferrite phase the sigma-phase transformation occurs at around 815 °C. Grade HL is otherwise similar to grade HK but its corrosion resistance is better as its chromium content is higher. [3]

Iron-nickel-chromium alloys, HN, HP, HT, HU, HW, and HX have nickel as their predominant alloying element. Due to their high nickel contents, their structures remain austenitic throughout their operating temperatures. [13] These alloys are considered susceptible to the formation of embrittling carbides. The formation of sigma-phase is not as common due to their high nickel contents. [3]

2.2.4 Mechanical properties

The mechanical properties of heat-resistant cast steels depend on numerous factors. For example the composition and the consequent microstructure of the steel have a great influence. This means that different grades of heat-resistant steels have different mechanical properties. The heat-resistant steel grades also differ from the grades of the corrosion-resistant steel series. Even greater differences occur between heat-resistant cast alloys and wrought alloys, as stated in Chapter 2.1.

Heat-resistant cast steels have high operating temperatures and therefore it is reasonable to study their mechanical properties at elevated temperatures. The mechanical properties at room temperature are almost irrelevant since they do not correlate with the properties at elevated temperatures. Properties of samples exposed to constantly high temperatures have a tendency to be better than those of the ones exposed to cyclic temperatures. [4]

In reference [4] a creep-rupture test was carried out on heat-resistant cast alloy HK-40 and wrought alloy 310 at 982 °C. The time-deformation curves of these alloys are shown in Figure 2.6. [4]

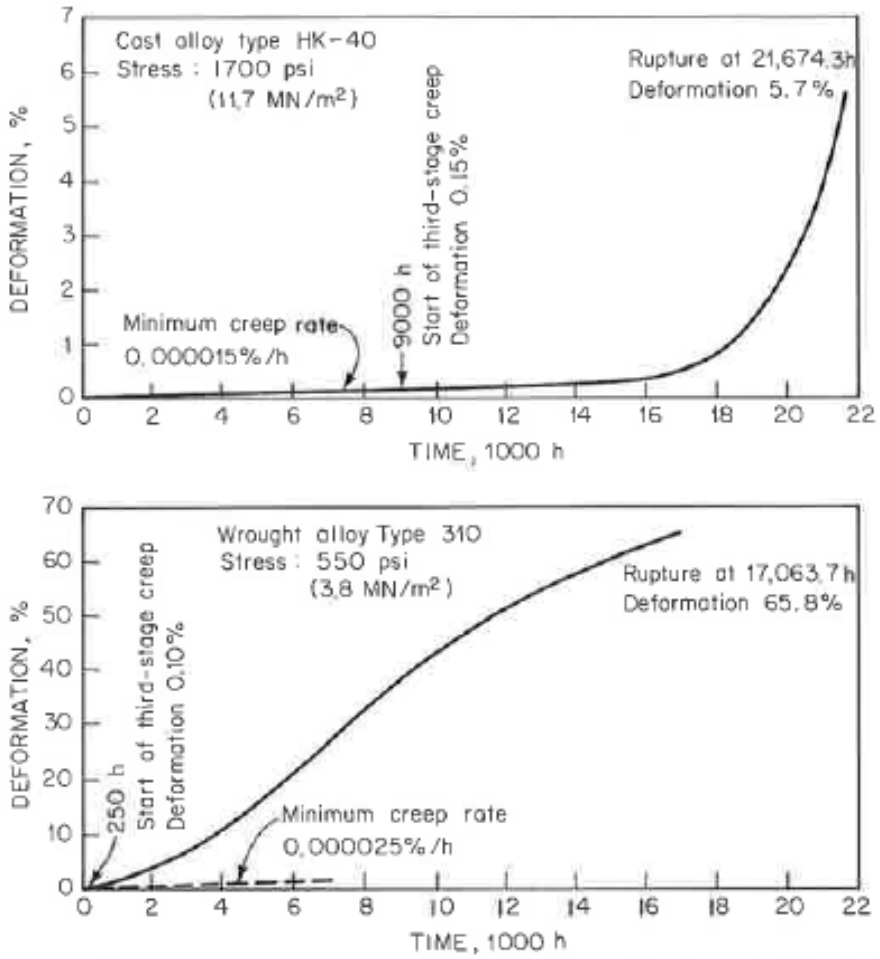

Figure 2.6. *The time-deformation curves for the creep-rupture test specimens of heat-resistant cast alloy HK-40 and wrought alloy 310 at 982 °C. [4]*

As can be seen in Figure 2.6, the cast alloy HK-40 has a remarkably smaller degree of deformation than the wrought alloy 310. It must be taken into account that the scale of deformation axis for the wrought alloy is ten times the scale of the cast alloy. Also noteworthy is that the applied loading stress for the wrought alloy is one third of the applied loading stress for the cast alloy. The times of rupture (in hours) do not differ as greatly as the degrees of deformation. There is a 91 % difference in the deformation degrees at rupture as compared to the difference in the times of rupture where it is only 21 %. The upper curve leads to the conclusion that the cast alloy HK-40 reaches its rupture point fairly soon after the material has started to deform significantly. This means that for this cast alloy, the deformation does not dictate the design stress as much as the time of rupture.

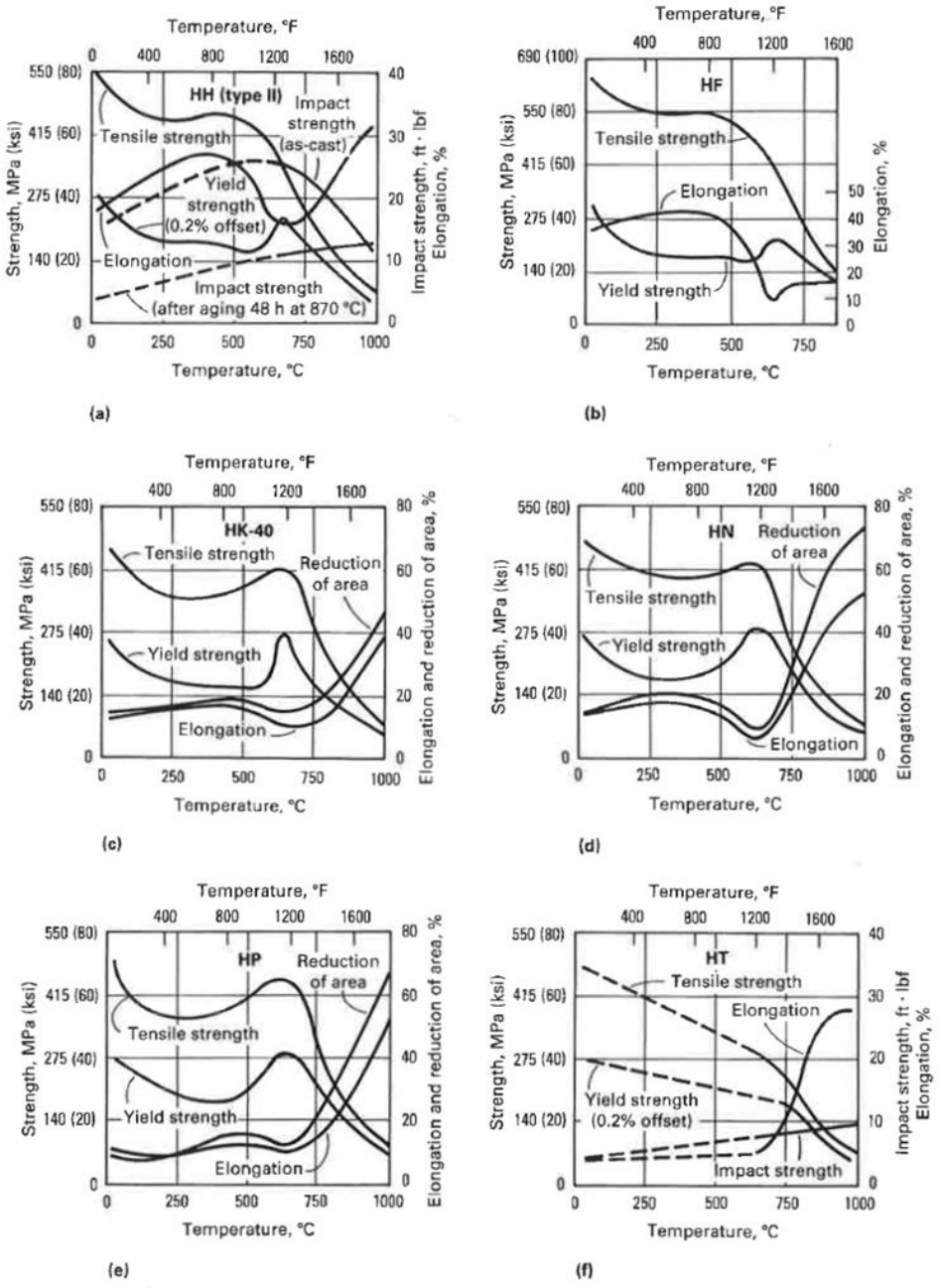

Figure 2.7. *The tensile properties of heat-resistant cast steels HH type II (a), HF (b), HK-40 (c), HN (d), HP (e), and HT (f) after short-term exposure to temperatures shown on the horizontal axis. [3]*

Figure 2.7 shows the tensile properties of six different grades of heat-resistant cast steels [3]. The properties were measured at room temperature after short-term aging. The common trend for all these grades is that their tensile strength values decrease with increasing aging temperatures. For grades HK-40, HN, and HP there is a definite increase in the tensile strength values before a drop at approximately 700 °C. Generally this type of increase in strength values is related to some kind of precipitation phenomenon, most probably to carbide precipitation. For the other grades HH type II, HF, and HT the curve is descending with increasing aging temperatures as well, though there is

no distinguishable sudden drop. The strengthening phenomenon of HK-40, HN, and HP is reduced in long-term aging. [3]

The trend of the yield strength values in Figure 2.7 is similar to that of the tensile strength values. There is an increase in yield strength followed by a clear drop after 650-700 °C for grades HK-40, HN, and HP. Elongations have a similar but opposite trend to the strength values. In all the grades in Figure 2.7 there are great variations in elongation with increasing aging temperatures, the elongations ranging from below 20 % up to above 50 %.

A noticeable feature for all heat-resistant cast steels is the changes in their mechanical properties in long-term aging. This is partly due to the precipitation of embrittling phases, such as sigma-phase. The precipitation of carbides and their dispersion in the structure may also have an effect. The embrittlement phenomenon is discussed in more detail in Chapter 3.

2.2.5 Corrosion behaviour

The corrosion behaviour of the heat-resistant cast steels is highly dependent on their chromium content. As stated earlier in Chapter 2.2.2, chromium reacts with oxygen and as a result those form a passive oxide film on steel surface. Figure 2.8 shows the corrosion behaviour of every heat-resistant cast steel grade. As can be seen from this figure, corrosion behaviour depends on the alloy type. [14]

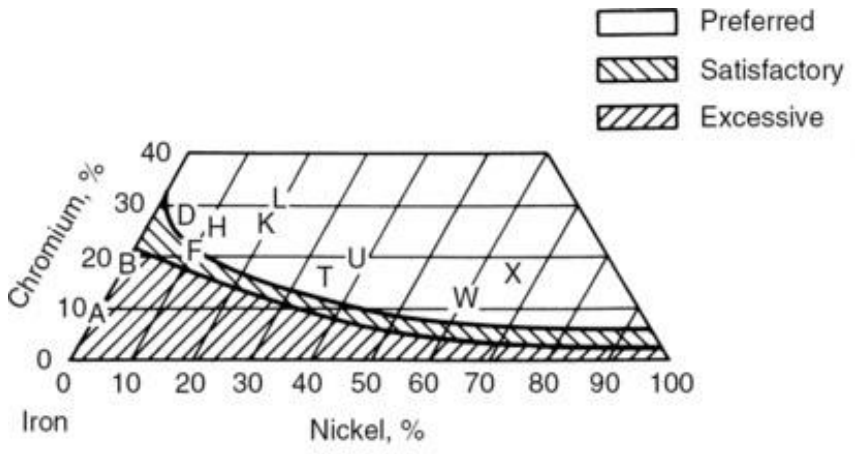

Figure 2.8. *The corrosion behaviour of heat-resistant cast steel grades in air. [14]*

Figure 2.8 indicates that the corrosion resistance is highest with the austenitic alloys HK and HL. Except for the ferritic alloys HA and HB, nearly all heat-resistant grades have corrosion resistance that is suitable for their applications at high temperatures in air.

Oxidation resistance is often measured by weight loss in percents. Cast stainless steels with chromium contents higher than 20% have high oxidation resistance. This means that their weight losses after exposing to high temperatures are small. The influence of chromium content on oxidation resistance is shown in Figure 2.9 as presented by weight loss percentages. The samples were exposed to 1100 °C for 48 hours. [14]

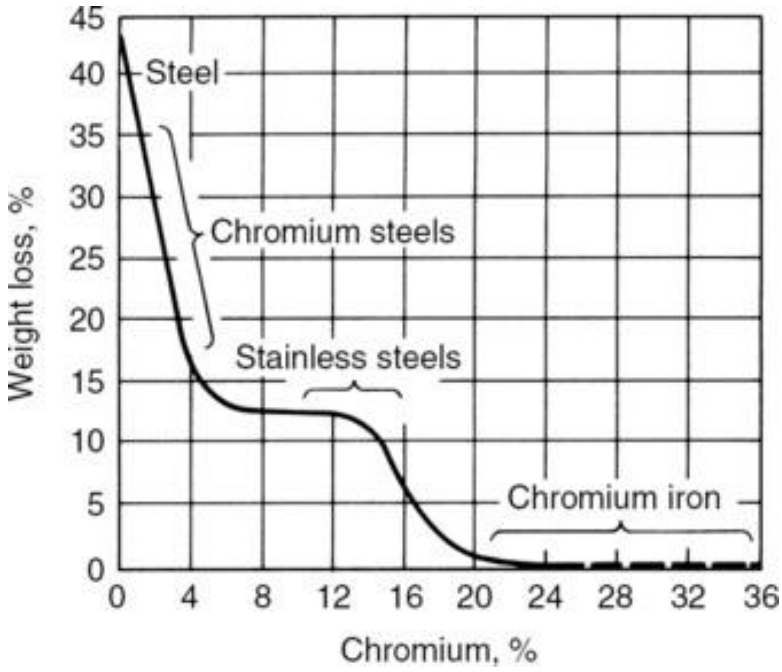

Figure 2.9. *The influence of chromium content on the oxidation resistance of casted steels as expressed by percentual weight loss. The samples were exposed to 1100 °C for 48 hours.[14]*

According to Figure 2.9 the weight losses reduce significantly as the chromium content increases. In practice this means that the oxide layer formed as a result of chromium reacting with oxygen is tightly adhered to the base material and does not crack easily.

3 EMBRITTLEMENT

Embrittlement decreases the ductility of the material. The ductility measures the degree of plastic deformation, which occurs before fracture. Ductile materials experience plastic deformation before fracture, while brittle materials fracture without plastic deformation. [5]

The embrittlement phenomenon is common for cast stainless steels at operating temperatures above 400 °C and below 1000 °C. These steels are susceptible to a variety of embrittlement phenomena. The 475 °C embrittlement is discussed only briefly in the following, since the operating temperatures of heat-resistant cast steels normally exceed 650 °C. Therefore the 475 °C embrittlement is not the key factor in the embrittlement of these steel grades. Other possibly embrittling factors, such as carbides, are also briefly presented. The main focus is on the sigma-phase embrittlement. [15]

475 °C Embrittlement

For stainless steels containing more than 13 wt% of chromium, the 475 °C embrittlement can cause the loss of ductility in the material. Iron-chromium alloys become harder and embrittled when held within the temperature range of 400-500 °C over a long period of time. The embrittling effect is most severe at 475 °C and because of that the phenomenon is called 475 °C embrittlement. The reason behind this embrittlement lies in precipitation hardening. Aging at temperatures near 475 °C leads to the formation of coherent precipitates consisting of chromium-rich solid solution. These precipitates also impair the corrosion resistance of the material, since they leave parts of the material chromium depleted. [15,16]

The 475 °C embrittlement does not exist with purely austenitic grades. Ferritic and ferritic-austenitic stainless steels on the other hand are susceptible to this impairing effect. Elongation to fracture can rapidly approach to zero. Also the impact strength can be reduced. At the same time hardness is increased tremendously. Treatment and operating temperatures between 400-550 °C should be avoided. Alternatively the chromium content of the material should be kept below the critical limit of 13 wt%. If embrittlement still occurs, it can be reversed by reheating the steel to 600 °C or above. Reheating restores the properties of the alloy. It can also induce the precipitation of the sigma-phase when carried out at higher temperatures. Therefore this treatment should be kept as brief as possible. [12,15]

Carbides

Unlike the corrosion-resistant cast steel grades, the heat-resistant grades have fairly high carbon contents ranging from 0.20 to 0.75 wt%. At temperatures above 650 °C, carbon is prone to react with chromium and form chromium-rich carbides of the type $M_{23}C_6$ (the letter M stands for metallic element, for example chromium). Normally these carbides have a strengthening effect and they are desired particles in Fe-Cr-Ni alloy microstructures. However, when exposed to elevated temperatures for longer periods, these precipitates may overage. This transition in the structure leads to the loss of creep resistance. [4] The dispersion of the carbides also influences the mechanical properties. When carbides are finely dispersed among the structure, strength is increased and ductility is decreased at room temperature. [1]

Precipitation of chromium carbides is extremely detrimental to corrosion resistance since chromium is no longer present in the surrounding structures. Chromium-free areas are formed near carbide particles leaving parts of the material susceptible to sensitization. [17]

Heat-resistant grades with lower carbon contents restrict the formation of chromium carbides by forming the iron-chromium compound known as the sigma-phase. Since the sigma-phase has highly adverse effects to the mechanical properties of the material, chromium carbides in the structure are favoured. By increasing the carbon content, the amount of chromium in the solid solution is reduced because chromium carbides are formed. This way the formation of the sigma-phase may be restrained. [18]

Sigma-phase

Sigma-phase has a tetragonal crystal structure. Its chemical composition is close to Cr_6Fe_7. [19] Each unit cell consists of 30 atoms. Sigma-phase is known to exist in over fifty binary systems. [18] In addition sigma-phase has been found in many ternary alloys as well. The hardness of sigma-phase in iron-chromium alloys is about 68 HRC. The presence of sigma-phase in the microstructure decreases ductility. Embrittlement is strongest at room temperature where specimens have been found to fracture even during hardness testing. [20]

Sigma-phase can precipitate in austenitic, ferritic, and ferritic-austenitic structures. [21] The composition of sigma-phase varies depending on the structure of the steel. Ferritic grades have a simple composition, whereas the composition of sigma-phase in austenitic grades is rather complex.

The influences of sigma-phase on the material can be highly detrimental. Reduction of toughness and ductility are the most critical effects of all. Problems in corrosion resistance may also occur, since sigma-phase is not resistant to oxidizing media. This is mainly an issue, which concerns alloys with intergranular sigma. Sigma-phase can also be finely distributed within the grains. In such cases it is possible that the presence of sigma phase increases the strength of the alloy. This, however, is rather uncommon since the sigma-phase usually precipitates at grain boundaries. [4] Chapters 3.1 and 3.2

study the formation of sigma-phase and its influences on the mechanical properties in a more specific manner.

3.1 The formation of sigma-phase

The formation of sigma-phase is undesirable. This phase is a hard and brittle iron-chromium intermetallic phase, which is formed when cast steel is aged in the temperature range of 650-870 °C. Besides temperature, sigma-phase formation depends also on time. Factors, which influence the sigma-phase formation, including the microstructure and composition of the material, are presented in more detail in Chapters 3.1.1-3.1.5. [4]

Sigma-phase forms more readily from ferrite phase than from austenite phase. The formation is fastest in ferritic iron-chromium alloys and in ferritic-austenitic alloys where the formation is mainly restricted to ferrite. There must be over 17 wt% of chromium in iron-chromium-nickel-based austenitic alloys in order for the sigma-phase to precipitate. In those alloys sigma-phase may precipitate directly from austenite. [20]

At first the sigma-phase nucleates at grain boundaries, between ferrite and austenite grains. Subsequently it grows into the ferrite phase. With increased aging time the sigma-phase particles grow in size and become coarse. According to the study of Garin et al. [19] the most preferable nucleation sites for sigma-phase are the ferrite-austenite phase boundaries (Figure 3.1a). This is the case especially with shorter aging times. When aging time is increased, the sigma-phase starts to grow into the ferritic phase (Figure 3.1b). In addition the sigma-phase starts to nucleate in the bulk of the ferrite phase.

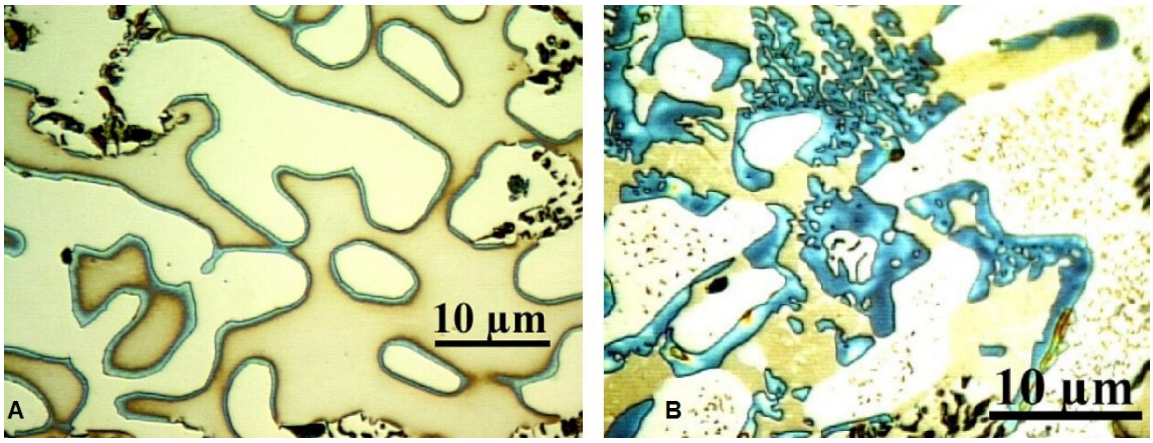

Figure 3.1a+b. *The formation of sigma-phase in HD-grade steel after annealing at 780 °C for 2 hours (a) and 48 hours (b). [19]*

In Figure 3.1a and Figure 3.1b the ferritic matrix is the yellow-coloured darker background and austenite grains are lighter yellow particles. Figure 3.1a shows the blue shade sigma-phase at ferrite-austenite phase boundaries. The influence of increased aging time is clear when the proportion of sigma-phase in Figure 3.1a is compared to that in Figure 3.1b.

The solution annealing is a heat treatment for austenitic and ferritic-austenitic stainless steels. This treatment is carried out at temperatures between 1040 and 1205 °C. When an alloy is heated to those temperatures all carbides and intergranular phases, including sigma-phase, will dissolve completely. The solution annealing is normally finished with water quenching. It is important to hold the alloy at the used temperatures long enough to accomplish the complete solution of the sigma-phase. Also quenching should be done at fast rate, since the carbides and other precipitates, such as the sigma-phase start to reprecipitate at temperatures between 540-870 °C. [1]

3.1.1 Temperature

The formation of sigma-phase is highly dependent on temperature. The temperature range where sigma-phase forms varies with composition. In general it can be stated that sigma-phase forms at temperatures from 565 °C to 980 °C. [18] Sigma-phase precipitation is generally fastest within the temperatures 700-810 °C. Composition and other factors such as processing slightly influence this temperature range. [16] In most cases the formation of sigma-phase can be eliminated by heat treatment at above 1000 °C. This annealing should be followed by moderate cooling. [22]

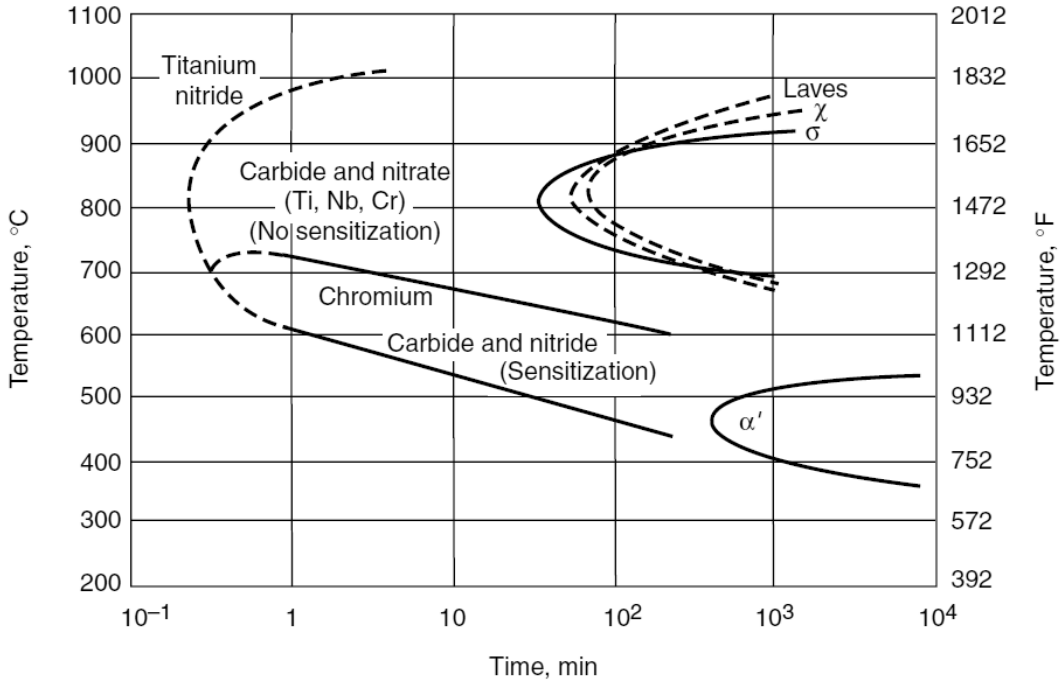

Figure 3.2. *Isothermal precipitation kinetics for carbides, nitrides, and intermetallic phases in ferritic alloys with 26 % chromium, 1-4 % molybdenum, and 0-4 % nickel. [10]*

Isothermal precipitation kinetics in ferritic alloys with 26 % chromium, 1-4 % molybdenum, and 0-4 % nickel are shown in Figure 3.2. The diagram shows that for this type of ferritic alloys the sigma-phase formation is fastest at temperatures close to 810 °C. At temperatures below 700 °C and above 900 °C the precipitation of sigma-phase is

slower. Notable is that the slowest formation time in Figure 3.2 is just above 1 000 minutes and that the precipitation is possible to start after only 50 minutes of heat treating. This is most likely due to the high chromium content of 26 %, which promotes the sigma-formation.

3.1.2 Time

The influence of time on the sigma-phase formation is evident. Similarly to temperature, also the time required for the precipitation of the sigma-phase depends on composition. In addition, prior working of the material has an influence on the time needed. It should be noted that the aging times are always dependent on the used temperatures. As stated earlier, the sigma-phase formation is generally fastest between temperatures 700 °C and 810 °C.

In general the sigma-phase precipitation occurs during long-term aging. However, the sigma-phase has been found in stainless steels after short-term aging as well. Chandra et al. [23] reported that ferritic-austenitic samples exposed to 900 °C for 15 minutes contained already ≈ 0.5 % sigma-phase. After 30 minutes of exposure to 900 °C there was over 2 % sigma-phase in the structure. About 3 % sigma-phase was present after 50 minutes of heat treatment. Approximately 20 wt% sigma-phase was observed when Garcés et al. [24] aged an as-cast sample of heat-resistant cast steel at 750 °C for 50 hours.

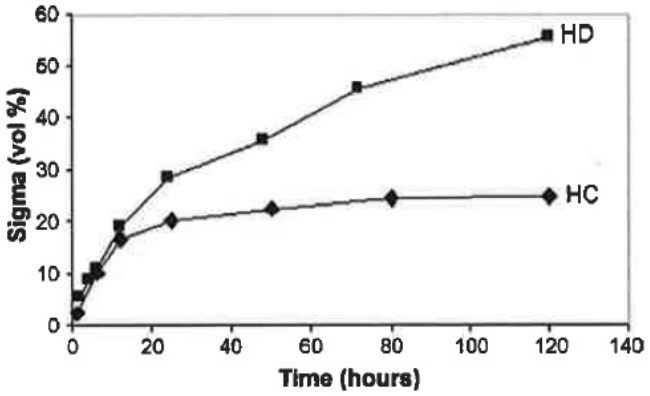

Figure 3.3. *The volume fraction of sigma-phase in heat-resistant cast steel grades HC and HD as a function of hours of heat treatment at 780 °C. [19]*

Garin et al. [19] exposed heat-resistant cast steel grades HC and HD to 780 °C. The volume fraction of sigma-phase in those steel grades is shown as a function of heating time in Figure 3.3. As can be seen in the figure, the content of the sigma-phase in grade HC stays almost constant at 20 vol% after 20 hours of heat treatment. On the other hand, in grade HD the sigma-phase content increases quite evenly throughout the test. This test indicates that in the studied steels fairly large amounts of sigma-phase can precipitate in less than 100 hours of heat treatment at 780 °C.

Time alone cannot determine the extent of the sigma-phase formation. It should be noted that there are several other factors, which influence the rate of precipitation as

well. Temperature and time play the key roles in the process, since they set the limit values for the other influencing factors such as microstructure and composition.

3.1.3 Microstructure

Microstructure in stainless steels can be austenitic, ferritic, ferritic-austenitic, or martensitic. The microstructures that are studied here are austenitic, ferritic, and ferritic-austenitic. Martensite is excluded from the list since none of the steel grades studied later on has a martensitic microstructure.

It is known that ferrite is more prone to sigma-phase formation than austenite. This is due to the ferrite-stabilizing elements, which promote the sigma-phase formation. However, sigma-phase does not form readily in pure iron-chromium alloys. Only when other alloying elements are added, the rate of sigma-phase formation is increased. In fully austenitic alloys the formation rate is rather slow. Ferrite-stabilizing elements, which are added to austenitic alloys, promote sigma-phase formation. The presence of delta-ferrite has the same accelerating effect on the precipitation rate. [18]

Besides the phase structure of the material, there are other microstructural factors, which influence the formation of sigma-phase in heat-resistant cast steels. According to Garcés et al. [24] the pre-existence of carbides in the steel can have an intense accelerating effect on the precipitation of sigma-phase. This is due to the high chromium content of these steels. The formed carbides may act as the source of chromium for sigma-phase. The study showed that there are differences in this behaviour between different types of carbides. The formation of sigma is faster from the Cr_7C_3 –type carbide than from the $Cr_{23}C_6$ –type carbide. This derives from the greater instability of the Cr_7C_3 compound at sigma-phase forming temperatures.

Schwind et al. [25] studied the sigma-phase precipitation in stabilized austenitic stainless steel AISI 321. Figure 3.4 shows the predictions and experimental data (marked as squares) for the sigma-phase precipitation at 700 °C.

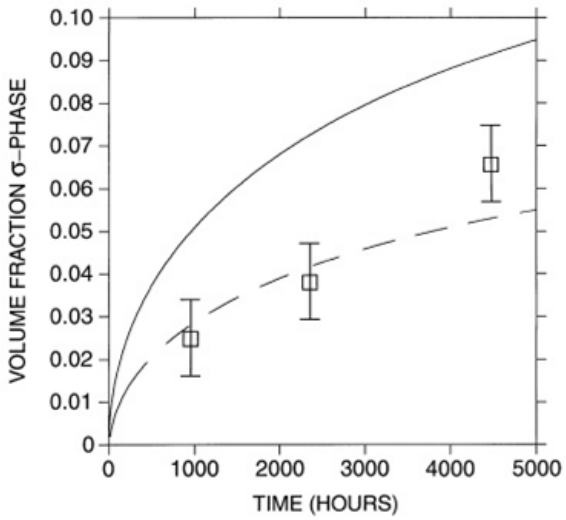

Figure 3.4. *The sigma-phase formation in a stabilized austenitic stainless steel AISI 321 as a function of aging time at 700 °C. [25]*

The solid line is obtained from a prediction of the sigma-phase formation using standard thermodynamic database, while the dashed line represents an evaluation by Lindholm [see 25, ref 9] where the influence of silicon on sigma-phase formation is also considered. As can be seen in Figure 3.4, the predicted amount of sigma-phase precipitation as a function of aging time is nearly equivalent to the experimental data. Since the studied material was stabilized, no formation of grain boundary carbides was observed. Most likely this was the reason for early precipitation of the sigma-phase. [25]

3.1.4 Composition

The composition of the steel has an enormous influence on sigma-phase formation. Garin et al. [19] found in their studies that alloying elements have an influence on both the rate of sigma-phase formation and the maximum amount of sigma-phase that can be formed. Generally alloying elements, which stabilize the ferritic phase, also promote the sigma-phase formation. Sims [26] indicated that the electron hole number $\bar{N}_v$ (equation (5)) may be used for predicting the formation of sigma-phase. With $\bar{N}_v \approx 2.50$ and below there were no signs of sigma-phase precipitation.

$$\bar{N}_v = 4.66\,(Cr + Mo) + 3.66\,(Mn) + 2.66\,(Fe) + 1.71\,(Co) + 0.61\,(Ni) \qquad (5)$$

As can be seen in equation (5), the elements, which stabilize ferrite, have higher coefficients in influencing the final value of $\bar{N}_v$. For austenite stabilizing elements, for example nickel, these coefficients are much lower.

Since the sigma-phase is an FeCr intermetallic compound, there needs to be chromium present in the steel alloy for the precipitation of sigma-phase. Usually the chromium contents in the sigma-phase containing alloys range from 25 wt% to 76 wt% [16]. With additional alloying elements the sigma-phase formation can occur in alloys with less than 20 wt% chromium [12]. Increasing the chromium content always enhances the sigma-phase formation. Carbon, on the other hand, has an opposite effect on the formation. In solid solution carbon has a high tendency to form carbides with chromium, hereby reducing the amount of chromium available for sigma-phase precipitation. At the same time these carbides may act as places for efficient sigma-phase nucleation. [18,20]

Both silicon and molybdenum favour the formation of sigma-phase. Only small additions of these elements can remarkably influence sigma-phase formation. As a ferrite stabilizer, aluminium somewhat accelerates the sigma-phase formation. The same effect can be achieved by adding small amounts of nickel and manganese. More radical additions have the opposite effect since they stabilize the austenitic phase and therefore the sigma-phase formation becomes decelerated. Tungsten, vanadium, and niobium promote the sigma-phase formation. According to two studies of Blachowski et al. [27,28] titanium significantly accelerates the formation of sigma-phase in iron-chromium alloys if the titanium content is smaller than 1.5 at%. The effect is the opposite with Ti-contents above 1.5 at%. [18]

3.1.5 Other factors

Prior annealing coarsens the grain structure of the steel. Sigma-phase formation is retarded by coarse grain sizes. This is due to the smaller amount of grain boundaries present in the structure. Since grain boundaries act as favourable nucleation sites for the sigma-phase, its formation is therefore retarded. Cold work has an opposite effect on the sigma-phase formation by enhancing it. However, the potential of cold work is highly dependent on its influence on recrystallization. Sigma-phase formation is enhanced if the amount of cold work is adequate to generate recrystallization at the operating temperature of the steel. If the amount of cold work is insufficient and recrystallization does not occur, the sigma-phase formation may actually be retarded. [18]

Chandra et al. [23] studied the sigma-phase formation in a duplex ferritic-austenitic stainless steel during and after hot working at 900 °C. The effects of hot working are shown in Figure 3.5 where curves (a) and (b) represent samples which have been deformed to a strain of 0.8 at strain rates (a) 1 sec^{-1} and (b) 0.01 sec^{-1}. Curve (c) represents the sample in undeformed state.

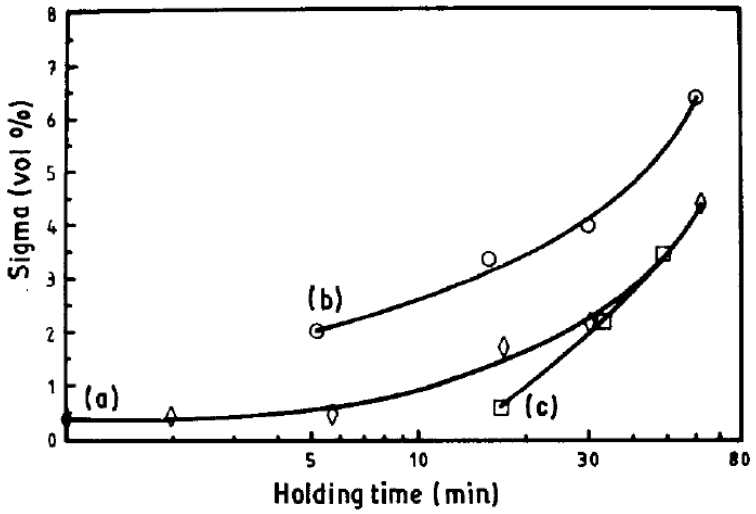

Figure 3.5. *The amount of formed sigma-phase (volume percentage) in a ferritic-austenitic duplex steel as a function of aging time at 900 °C in hot worked (a, b) and undeformed (c) samples. In curve a) the deformation rate during hot working is 1 sec^{-1} and in curve b) it is 0.01 sec^{-1}. [23]*

As can be seen in Figure 3.5, the formation of sigma-phase is enhanced by hot working at 900 °C. This is due to the deformation of the material; it induces lattice defects which act as favourable nucleation sites for sigma-phase. According to the study, the samples deformed at lower strain rate of 0.01 sec^{-1} contained more sigma-phase than the samples deformed at the higher strain rate of 1 sec^{-1}. The reasons lie in dislocations, in their density and velocity. Deformation at higher strain rates results in higher dislocation density. This means that there will be fine sigma-phase precipitates throughout the structure. However, the dislocation velocity will be higher at higher strain rates. High dislocation velocity is linked to lower growth rate of sigma-phase particles, since the sigma-phase

particles are in contact with individual dislocations for shorter time periods. All in all, samples deformed at higher strain rates have plenty of fine sigma-phase particles but the total volume fraction of sigma-phase is greater in samples deformed at lower strain rates. [23]

3.2 The influence of sigma-phase on mechanical properties

Sigma-phase itself is hard and brittle. Therefore its effects on mechanical properties can be extensive. Heat-resistant cast steels exposed to operating temperatures of 650-800 °C are susceptible to the sigma-phase formation. For that reason material selection is extremely important.

The mechanical properties of heat-resistant cast steels were studied briefly in Chapter 2.2.4. In this chapter the focus is on the changes of mechanical properties caused by the sigma-phase formation. These changes are most evident at room temperature. Impact strength and hardness will be covered more extensively, since those are the properties which were measured later in the experimental part of the thesis.

3.2.1 Impact strength

The ability of a material to resist shock loading is measured by its impact energy or impact strength [29]. This measure differs from tensile strength since it measures the maximum energy absorbed during the fracture in shock loading. The tensile strength is measured under low and steady loading rate, for example in a tensile test. Impact strength measurements are carried out by using specimens with standard dimensions [5]. Most known test types are Charpy and Izod impact tests which differ from each other by the positioning of the test specimen. Charpy impact test is discussed more in Chapter 5.3.

The impact strength is the most sensitive mechanical property, which is influenced by sigma-phase. A study was made on the toughness of a Fe-25Cr-20Ni alloy by Emanuel [see 18, ref 225]. He discovered a significant loss in toughness due to the sigma-phase. In his study the samples were aged at temperatures ranging from 550 °C to over 900 °C for up to 3000 hours.

Figure 3.6 shows that the influence of aging on toughness increases as the aging time increases. There is also a significant drop in the impact energy at temperatures above 650 °C. However, the toughness is restored when the alloy is heated up to temperatures of 900 °C and above. At those temperatures the original microstructure of the Fe-25Cr-20Ni alloy is recovered and the sigma-phase is vanished.

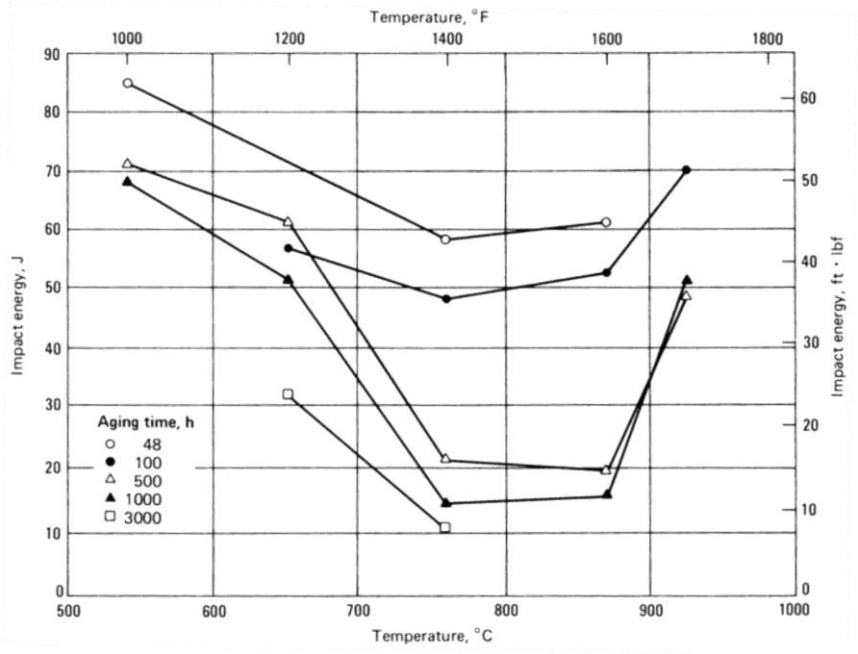

Figure 3.6. *The room-temperature impact energy of the alloy Fe-25Cr-20Ni as a function of aging time and temperature. [see 18, ref 225]*

It should be noted that heat-resistant cast steels have more carbon as an alloying element than the alloy Fe-25Cr-20Ni. Carbon is known to strengthen the alloy, but at the same time it is prone to react with chromium. This reaction results in chromium carbides which can also act as a major factor in decreasing the impact strength of the material.

Aggen et al. [see 18, ref 226] found that the impact energies of the 29Cr-4Mo ferritic stainless steel samples mainly decreased with increased aging time and temperature. Room-temperature impact energies of those samples aged at different temperatures are shown in Figure 3.7 as a function of aging time.

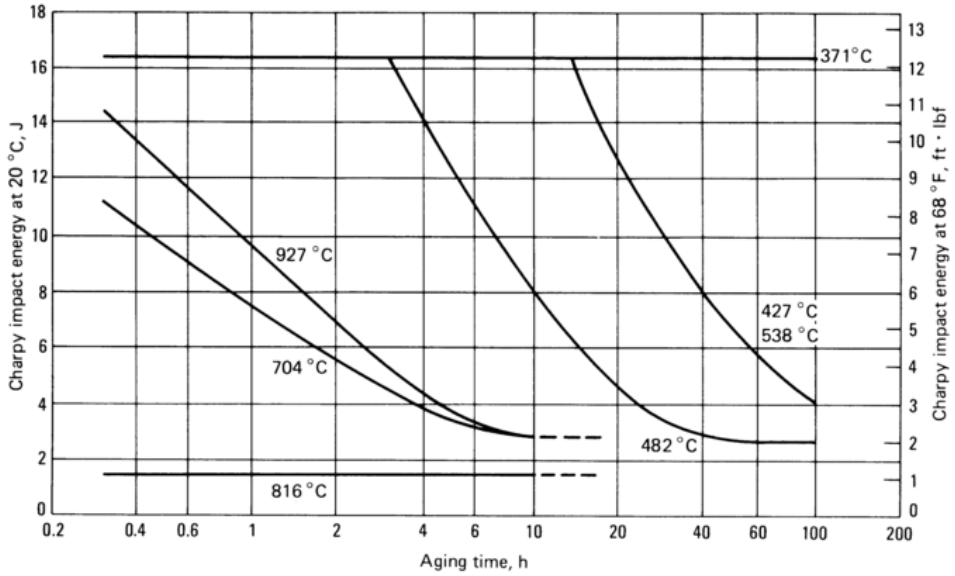

Figure 3.7. *The influence of aging time on room-temperature impact energy of ferritic stainless steels samples aged at temperatures between 371-927 °C. [see 18, ref 226]*

Curves related to the sigma-phase are the ones measured after aging at temperatures 704 °C, 810 °C, and 927 °C. Aging at 704 °C has a decreasing influence on impact energy as aging time increases. Regardless of the aging time, aging at 816 °C embrittles the alloy completely. The influence of aging at 927 °C is similar as at 704 °C. These curves indicate, as stated previously, that the sigma-phase formation rate is highest at temperatures near 800 °C. [18]

Aging at temperatures 427 °C, 482 °C, and 538 °C produced decrease in impact energy of the ferritic stainless steel samples. Here the embrittlement phenomenon is 475 °C embrittlement, which is common for ferritic stainless steels. Aging at 371 °C did not result in any loss of toughness. [18]

3.2.2 Hardness

The resistance of a material to local plastic deformation is measured by its hardness. Earlier material hardness was qualitatively analysed by rubbing two materials against each others. If the material was able to scratch the other, it was harder and the scratched material softer. These days different quantitative techniques are used. These are based on the indentation hardness of the material. A small indenter is pushed into the surface of the material under controlled load and rate. This results in an indentation trace which is measured by depth or size. The size of the indentation diminishes as the hardness increases. In addition to the test based on indentation, other hardness test methods are used as well. [5]

Hardness significantly increases as sigma-phase forms, since the phase itself is extremely hard with Rockwell C hardness of approximately 68 HRC (equivalent to Vickers hardness of 940 HV and Rockwell B hardness of 816 HB). Garin et al. [19] discovered increase in hardness as the relative content of sigma-phase increased in the heat-resistant cast steel grades HC and HD. This is shown in Figure 3.8.

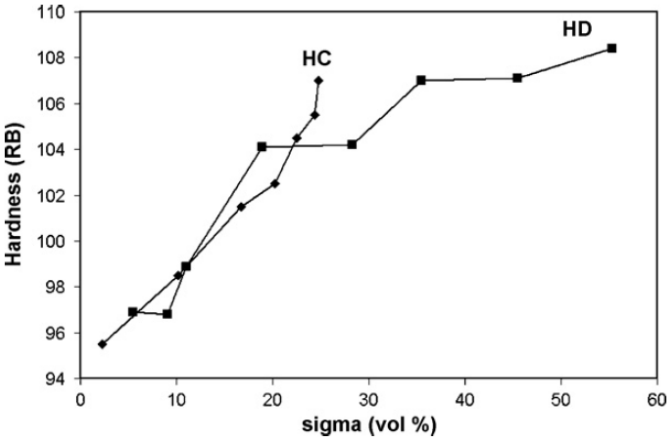

Figure 3.8. *Hardness (Rockwell B) of the heat-resistant cast steel grades HC and HD as a function of sigma-phase content. [19]*

For grade HC the increase in hardness with increasing sigma-phase content is steeper than for grade HD. However, the differences in hardness are only about four percent at

sigma-phase content of 25 vol%. Grade HD clearly verifies the correlation between hardness and sigma-phase content. The same applies also to grade HC.

The effects of aging at 750 °C on the hardness of an austenitic stainless steel were studied by Rodríguez et al. [30]. Samples of the cast heat-resistant alloy KHR45 (0.39 C, 1.30 Si, 0.84 Mn, 33.1 Cr, 20.2 Fe, 0.42 Nb, Ni bal. wt%) were aged at 750 °C for six weeks (1008 h). The study showed no clear evidence of the sigma-phase formation. This most likely is due to the high nickel content of the alloy.

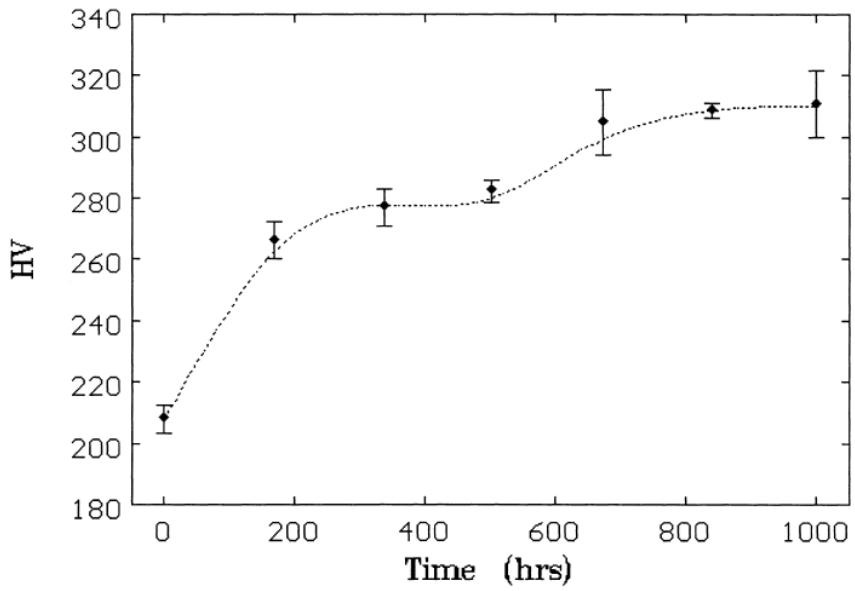

Figure 3.9. *Variation of hardness (Vickers) as a function of aging time of the cast heat-resistant steel KHR45 samples aged at 750 °C. [30]*

Figure 3.9 shows the variation of Vickers hardness in the steel KHR45 as a function of the aging time. There is a definite increase in the hardness values. In this case the increase does not result from the sigma-phase formation. The reason here lies in the formation of hard carbide particles that precipitate during aging.

The previous two studies of Garin et al. [19] and Rodríguez et al. [30] are presented here even though the focus in both articles is not on the sigma-phase. Garin et al. focus more on hardening due to the sigma-phase, whereas the study of Rodríguez et al. concludes that the carbide particles are the primary cause for hardening. It is important to note that the hardening as a result of aging is not automatically caused by the formation of sigma-phase. As Rodríguez et al. showed in their study, another convincing reason for the increase in hardness is the precipitation of hard carbides. Since there are two significant factors that can cause the increase in hardness, it is essential to study also the microstructure in order to confirm the structural cause for hardening.

3.2.3 Strength

Tensile strength is the maximum stress a material can sustain under tensile load without fracturing. Prior to this maximum applied stress, the tested material has already started

to deform uniformly. At the maximum stress point the deformation will localize on some point of the specimen and a neck will begin to form. Typical tensile strength values of heat-resistant cast steels range from 450 N/mm^2 to almost 800 N/mm^2. These values are normally increased after aging treatment. [1,5]

At elevated temperatures the tensile properties decline. Figure 2.7 on page 12 shows this decrease of tensile strength values in heat-resistant cast steels. Lopez et al. [31] studied the influence of sigma-phase on the mechanical properties of ferritic-austenitic stainless steels. In their study slow strain rate tests (SSRT) were performed in different environments. A typical curve from SSRT in inert environment is presented in Figure 3.10.

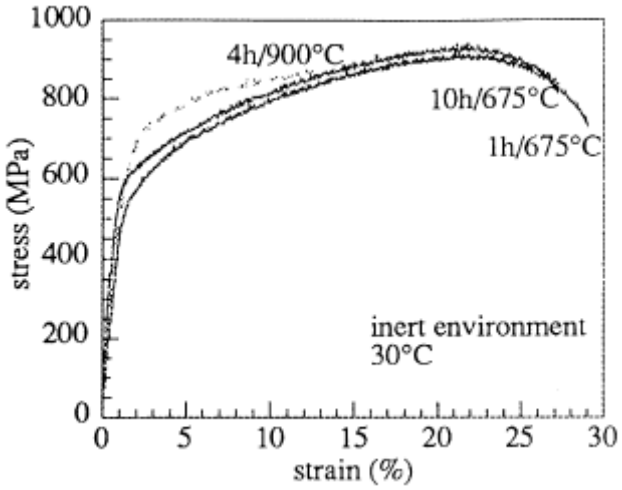

Figure 3.10. *The stress-strain curves of ferritic-austenitic duplex stainless steels after different aging treatments as measured with slow strain rate tensile test at 30 °C in inert environment. [31]*

Lopez et al. found in their study that most likely the presence of sigma-phase markedly influences the mechanical properties of duplex stainless steels. However, it should be noted that this deterioration can also result from the carbide formation. The heat treatments in this study were carried out at temperatures 675 °C and 900 °C. Both treatments resulted in the formation of sigma-phase. Another conclusion of this study was that sigma-phase affects intergranular corrosion. Reductions of corrosion resistance are discussed in Chapter 3.3.1.

3.3 Effects of sigma-phase on other properties

In addition to mechanical properties, sigma-phase also influences other material properties. Effects on corrosion resistance and elevated-temperature properties are covered here only shortly, since in this work the real concern with sigma-phase is always the decline in ductility.

3.3.1 Resistance to corrosion

The corrosion resistance of heat-resistant cast steels varies greatly with alloy type. However, all cast stainless steels suffer a reduction in corrosion resistance, if the sigma-phase is a part of their structure. The effects of sigma-phase are slightly different in austenitic and ferritic steels.

In austenitic stainless steels the sigma-phase may lead to intergranular corrosion. This is due to the relatively continuous networks of sigma-phase at grain boundaries. Studies have also shown that sigma-phase can increase the susceptibility to intergranular corrosion, even when it is not yet visible in optical microscope. Highly alloyed steel grades can also suffer from pitting and crevice corrosion due to the precipitation of sigma-phase. Resistance to corrosion will reduce severely in highly oxidizing environments, such as nitric acid HNO_3. Only small amounts of sigma-phase are needed to reduce corrosion resistance. [10]

Ferritic stainless steels suffer from the reduction in corrosion resistance as well as the austenitic ones. Sigma-phase that precipitates in grain boundaries as continuous networks is considered to be more detrimental than separate sigma-phase precipitates. Altogether the presence of sigma-phase can also diminish the corrosion resistance of the material since it has higher chromium content than ferrite. Therefore the matrix phase is left chromium depleted, especially around sigma-phase precipitates. This, however, is not considered the main reason for the loss in corrosion resistance. [10]

Corrosion resistance is always reduced due to the formation of the sigma-phase. It should be kept in mind that the reason behind this reduction cannot necessarily be explained by chromium depletion mechanism as in most cases with stainless steels. Sigma-phase itself exposes the material to localized corrosion. However, how severe the decrease in corrosion resistance due to the formation of sigma-phase may be, the embrittlement is always considered as the most detrimental effect without exception. [10]

3.3.2 Elevated-temperature properties

The elevated-temperature properties of heat-resistant cast steels are generally good, since those steels were developed for the use at temperatures over 650 °C. A few studies [32] have shown that sigma-phase can be beneficial for alloys used in applications involving erosion or wear at elevated temperatures. This is due to the hardening effect caused by the sigma-phase. Usually this increase in hardness is retained also at lower temperatures. At the same time toughness, however, is decreased. Therefore the operating conditions and requirements should be considered carefully before deciding whether the sigma-phase may be beneficial or not. [32]

The embrittling effect of sigma-phase is always greatest at room temperature. Toughness and ductility are better preserved in sigma-phase containing steels at high temperatures. It should be noted that the sigma-phase may not necessarily be the only embrittling phase present in the microstructure. Exposures to high temperatures can

result in a variety of different phases that may affect the properties. Even so the sigma-phase is usually the most likely cause for the loss of ductility. [32]

4 AIM OF THE STUDY

The formation of sigma-phase in heat-resistant cast steels is an undesired phenomenon. Since the sigma-phase is a hard and extremely brittle phase, its presence in the microstructure embrittles the material. The embrittlement is strongest at room temperature. Even though the heat-resistant cast steels are designed mainly for the use at elevated temperatures, the operating conditions may include also, for example, maintenance or repair at room temperature. Therefore the formation of sigma-phase and its influences should be studied widely.

This study is a part of DEMAPP (Demanding Applications) Melt project. The focus in DEMAPP is on the demands for materials in extreme conditions. The aim in this part of the project is to find out how much sigma-phase is formed during different aging times and to study the factors that influence the sigma-phase formation. The influences of sigma-phase on mechanical properties are also studied.

In this study the test materials were aged at a temperature of 820 °C for different periods of time; 100, 300, 600, and 1200 hours. After long-term aging the samples were prepared for microstructural characterisation. The as-cast samples were also characterised. The purpose was to study how much sigma-phase will precipitate in the samples aged at 820 °C for different time periods. Since the materials varied in their microstructures and compositions, the presumption was that there would be great differences in the amount of precipitated sigma-phase.

In addition to determining the amount of precipitated sigma-phase, the mechanical properties were also studied. Numerous studies have shown that the formation of sigma-phase has an influence on the mechanical properties of the material. Especially impact toughness and hardness are affected. These properties were studied in more detail.

The overall aim of this study was to determine the amount of sigma-phase, which precipitates in heat-resistant cast steels of different grades at different aging times at the constant temperature of 820 °C. The focus was on determining the correlation between the amount of precipitated sigma-phase and its influence on impact toughness and hardness values.

The experimental part is presented in Chapters 5, 6, and 7. The measurements and characterisation support the theoretical background presented in Chapters 2 and 3.

5 TEST MATERIALS AND METHODS

5.1 Materials and chemical compositions

Test materials were cast at Valimoinstituutti. Three of the test materials were standard grades of heat-resistant cast stainless steels (see Chapter 2.2.3). A slightly modified HD steel belongs to the iron-chromium alloys whereas the two standard steels HH and HI belong to the iron-chromium-nickel alloys. The compositions of the test materials are presented in Table 5.1.

Table 5.1. *The test materials and their chemical compositions.*

	Cr	Ni	C	Mn	Si	Mo	N	S	P	Cu	Al	Fe
HH (a)	25.51	12.68	0.30	1.48	1.27	0.28		0.01	0.01	0.12	0.01	58.16
HH (b)	24.92	12.16	0.41	1.15	1.22	0.37		0.01	0.03	0.00	0.00	59.73
HD	27.00	6.40	0.47	1.06	2.86	0.37	0.42	0.01	0.02	0.06	0.01	61.32
HI	25.70	16.50	0.38	1.03	1.37	0.21		0.00	0.02	0.20	0.01	54.32

The compositions shown in Table 5.1 are the actual compositions of the test materials. They do not markedly differ from the target compositions, which were set in the middle of standard limits. There are two sets of grade HH that are marked differently – HH (a) and HH (b). HD material differs slightly from the standard version of HD steel due to the additions of nitrogen and silicon.

Test materials were received in as-cast condition. Figure 5.1 shows an example of a test material piece in as-cast condition. These cast samples were sawed into smaller specimens in order to fit them into the chamber furnace for the heat treatment process. The specimens were sawed from the middle parts of the castings with the aim of receiving as dense specimens of the material as possible.

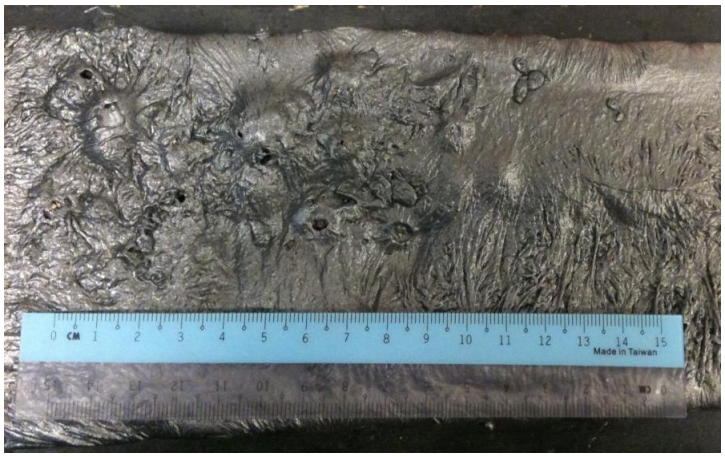

Figure 5.1. *Example of a test material in as-cast condition.*

5.2 Long-time exposure at elevated temperatures

Heat-resistant steel specimens were exposed in a heat treatment process (aging) which was carried out in air atmosphere in a laboratory chamber furnace (Lenton EF 11/8) at 820 °C. Test series consisted of four sets of different aging times, each containing three specimens of each steel grade - 48 specimens in total. The aging times were 100 h, 300 h, 600 h, and 1200 h. The specimens were placed in ceramic crucibles and the crucibles were fitted into the chamber. Due to the limited volume of the chamber, four crucibles were fit inside at a time.

At first the specimens of 100 h and 1200 h aging were placed in the chamber. After 100 hours of aging the specimens of 100 h were taken out and 300 h specimens were placed into the chamber. The same procedure was repeated with 300 h and 600 h specimens. At the end part of the heat treatment there were only the specimens of 1200 h left in the chamber.

5.3 Test methods for impact toughness measurements

Aged steel specimens were machined into Charpy V-notch impact test bars. The size of these test bars was 55 mm x 10 mm x 10 mm according to the standard ASTM A370 (Standard Test Methods and Definitions for Mechanical Testing of Steel Products). The test bars were finalized by machining the V-notch with root radius of 0.25 mm (in Figure 5.2). [33,34]

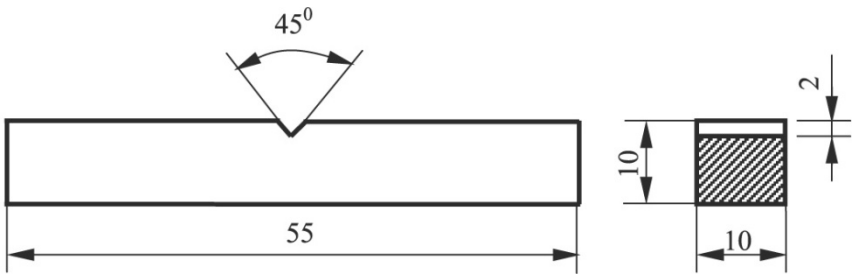

Figure 5.2*. The Charpy V-notch impact test specimen according to the standard ASTM A370. [34]*

In Charpy impact testing the notched specimen is struck by a special pendulum hammer. The aim is to break the notched specimen by a single stroke. Figure 5.3 is a simplified presentation of the Charpy impact testing machine. In the beginning of the test, the pendulum hammer is lifted to the starting position. Then the test specimen is placed carefully against anvil so that the V-notch is positioned in the middle. Finally the hammer is let loose. The hammer hits the middle section of the specimen on the opposite side of the V-notch when reaching its lowest position. The energy consumed in breaking the sample can be calculated from the height difference between the initial position and the end of swing position of the hammer after breaking the sample. The

consumed energy is usually converted into joules and can be observed directly from the device scale.

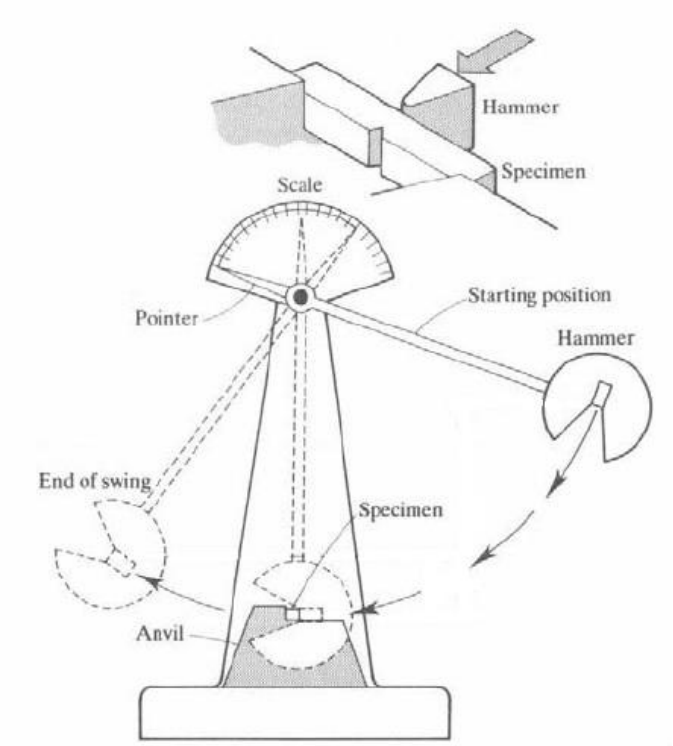

Figure 5.3. *The Charpy impact testing machine and the positioning of the test specimen. [35, simplified]*

The impact strength tests were carried out by using two Charpy impact machines of different scales. As-cast and 100 hours aged specimens were tested at room temperature using Charpy impact machine of 300 J. The testing of 300, 600, and 1200 hours aged specimens was also carried out at room temperature but using a smaller Charpy impact machine of 50 J. The reason for using two different test machines was maintaining an adequate accuracy in reading the scale.

5.4 Test methods for hardness testing

The Vickers hardness test was applied in measuring the hardness values of the test samples. In Vickers hardness test a tiny diamond indenter is pressed against the sample surface. This indenter has the shape of a pyramid, as shown in Figure 5.4. The diagonals of the produced indentation are measured. Finally the hardness is calculated using the formula for Vickers hardness number shown in equation (6). [5]

Figure 5.4. *The shape of the diamond indenter used in Vickers hardness testing. [5]*

In the equation (6) the Vickers hardness number is calculated as a function of applied load P and the average length of the two indentation diagonals d_1. [5]

$$HV = 1.854P/d_1^2 \quad (6)$$

In this study, three kilogram load was used. In total ten measurements were taken from each test sample. The final Vickers hardness numbers shown in Chapter 6.2 are average values of these ten measurements.

5.5 Test methods for microstructural characterisation

Test samples were prepared for microstructural characterisation via a set of definite sample preparation steps. This sample preparation was carried out to reveal the microstructure. First the samples were ground and polished as shown in Table 5.2.

Table 5.2. *Sample grinding and polishing steps for optical microstructural characterisation.*

Stage	Step	Time [min]
Grinding	SiC-Paper #120	2
Grinding	SiC-Paper #220	2
Grinding	SiC-Paper #340	2
Grinding	SiC-Paper #600	2
Grinding	SiC-Paper #800	2
Grinding	SiC-Paper #1200	2
Grinding	SiC-Paper #2500	2
Grinding	SiC-Paper #4000	2
Polishing	Napless Cloth, 3 µm diamond suspension	2
Polishing	Soft Cloth, 1 µm diamond suspension	2

After each step the samples were rinsed with water and ethanol and dried carefully with a drier.

Grinding and polishing was followed by electrolytical etching of the test samples. There are several possible etchants for heat-resistant steel grades. In this study oxalic acid and sodium hydroxide were used. The test samples were electrolytically etched (Struers LectroPol-5) using the voltage of 4.5 V (oxalic acid) and 3.0 V (sodium hydroxide). Etching times varied from five to ten seconds.

5.5.1 Optical Microscopy

All electrolytically etched specimens were studied using optical microscope (Leica DM 2500M). Optical micrographs are presented in Chapter 6.3.1. Objective magnifications of 10x and 50x were used.

At first all polished specimens were electrolytically etched with 10% oxalic acid to reveal the microstructure. As Chapter 6.3.1 later shows, this etchant did not stain any phases with different colours. However, the overall microstructure was revealed as a result.

In order to reveal the differences between the sigma-phase and the rest of the microstructure, the as-cast specimens as well as the 100 and 1200 hours aged specimens were electrolytically etched with 20% sodium hydroxide (NaOH). These specimens were chosen, since they showed the greatest changes in their impact toughness values (see Chapter 6.1).

5.5.2 SEM + EDS studies

After sample preparation the microstructures of the as-cast and 1200 hours aged specimens were studied using scanning electron microscope (SEM) Philips XL-30 and attached energy dispersive spectroscope (EDS) EDAX DX4 for compositional analyses (see Figure 5.5). SEM studies were conducted using both secondary electrons (SE) and back-scattered electrons (BSE). Different phases were analysed using EDS. The results of SEM + EDS studies are presented in Chapter 6.3.2.

SEM studies consisted of imaging the microstructures. Several images were taken. EDS analyses were taken from several different phases. The results of these analyses are discussed in Chapter 7.3.2.

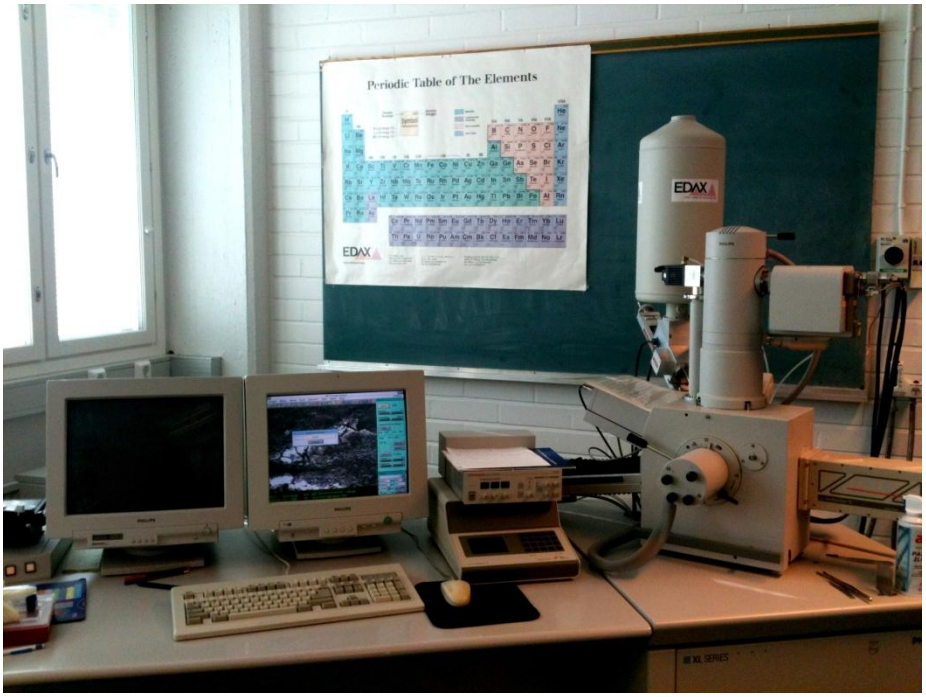

Figure 5.5. *SEM + EDS equipment used in this study.*

6 RESULTS

The results of the experimental part of this study are presented in this chapter. Results of the studies on mechanical properties are presented first in Chapters 6.1 and 6.2. Chapter 6.3 presents the results of microstructural characterisation: optical microscopy, SEM studies and EDS analyses.

6.1 Impact toughness

Impact toughness values were measured for each studied steel grade (HH (a), HH (b), HD, and HI). Each grade had five sets of three samples. The samples of each set were aged at 820 °C for different times: 100, 300, 600, and 1200 hours. For each steel grade – aging time combination three samples were tested at room temperature and the final impact toughness value was calculated as the average of the three test results. In addition, one set consisted of as-cast samples. Impact toughness values were measured from 60 samples in total. The results of these measurements are shown in Figure 6.1.

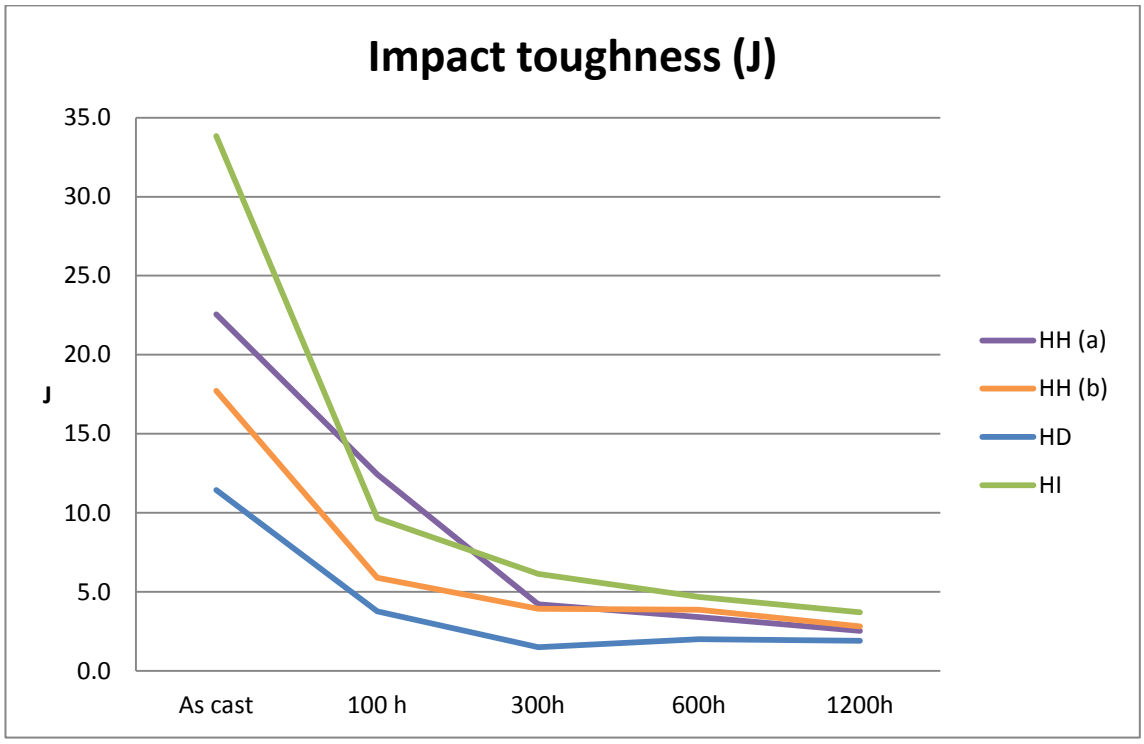

Figure 6.1. *The room temperature impact toughness values (in Joules) of the studied steels HH (a), HH (b), HD, and HI as a function of hours aged at 820 °C.*

6.2 Hardness

Vickers hardness was measured for each grade (HH (a), HH (b), HD, and HI). Each grade had five different samples: as-cast and samples aged for 100, 300, 600, and 1200 hours at 820 °C. Ten measurements were taken from each sample and the final hardness value was calculated as the average of the ten results. In total 200 measurements were taken. The results of these measurements are shown in Figure 6.2.

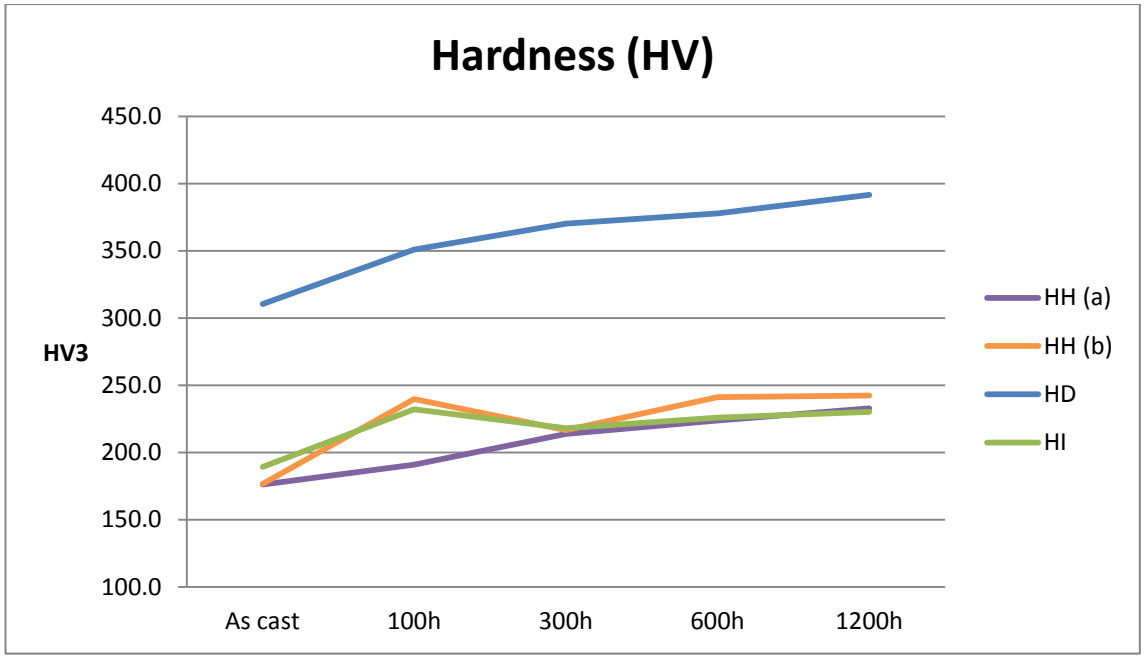

Figure 6.2. *The Vickers hardness values (in HV3 units) of the studied steels HH (a), HH (b), HD, and HI as a function of hours aged at 820 °C.*

6.3 Microstructural characterisation

Microstructural characterisation of the samples consisted of two individual characterisation techniques. At first the microstructures were studied using optical microscope. These studies were made for all samples electrolytically etched with oxalic acid. In addition, the samples electrolytically etched with sodium hydroxide were also studied. The sample preparation is presented earlier in Chapter 5.5.

The SEM + EDS studies were carried out on electrolytically etched samples in as-cast and 1200 hours aged conditions. The samples used in these studies were all etched using oxalic acid as the etchant.

6.3.1 Optical Microscopy

Optical microscopy images were taken for all electrolytically etched samples. In general, the images showed significant changes in microstructures as a function of aging hours. The microstructures of different grades were also compared with each other and the structures showed differences.

Images taken from the samples electrolytically etched with oxalic acid are presented in Figures 6.3 - 6.6. The images are presented in the following order (see Table 6.1).

Table 6.1. *Corresponding image labels and sample conditions on the samples electrolytically etched with oxalic acid.*

Label on the image	Sample condition
A, B	as-cast
C, D	aged for 100 hours
E, F	aged for 300 hours
G, H	aged for 600 hours
I, J	aged for 1200 hours

Images were taken using different magnifications. The images shown on the left side of the figures were taken using objective magnification of 10x, the ones on the right side using objective magnification of 50x. There is a scale bar in every image to show the true magnification.

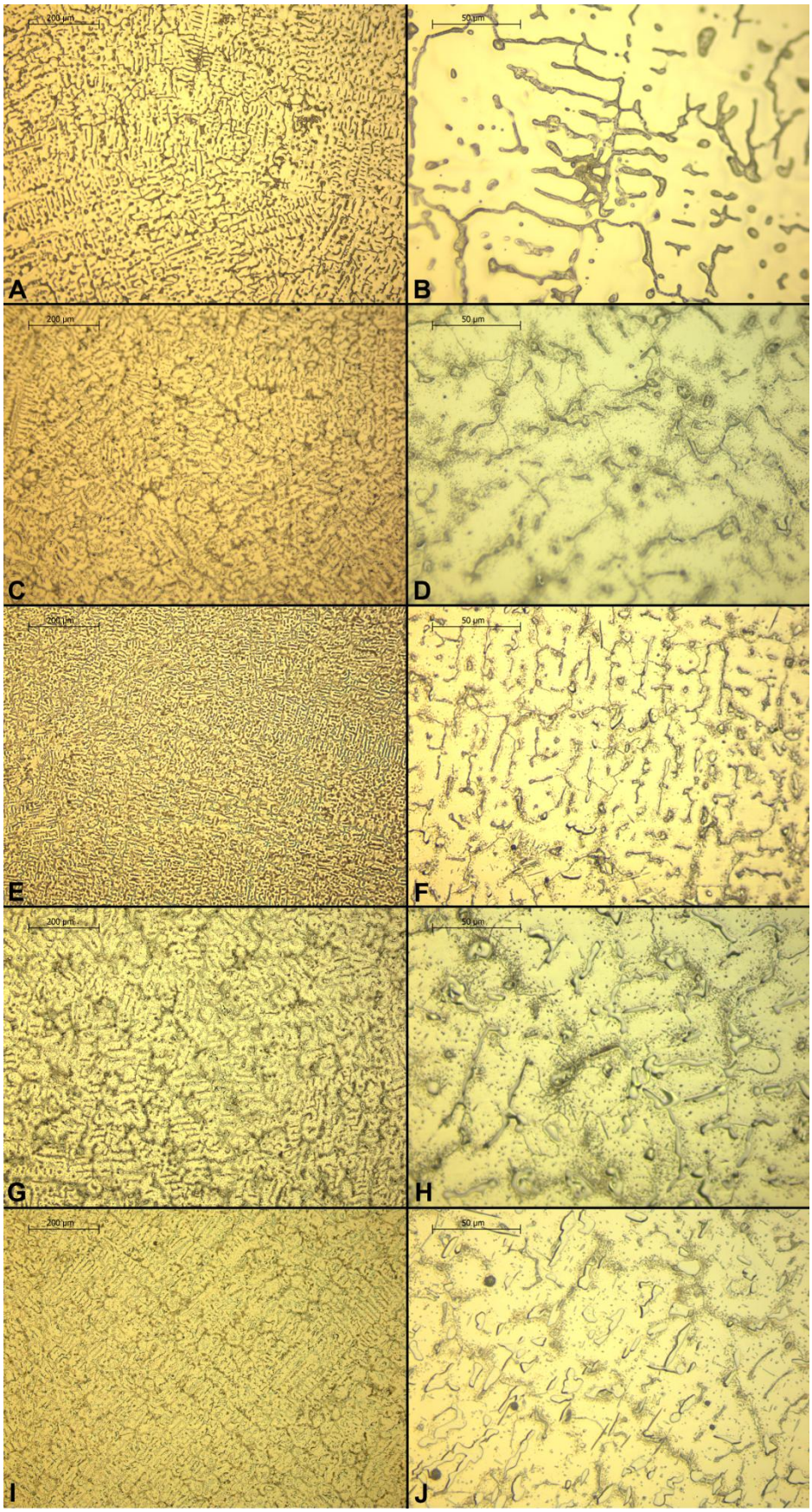

Figure 6.3. *Optical microscopy images of the steel HH (a), where A and B are of as-cast sample, C and D of 100 hours aged, E and F of 300 hours aged, G and H of 600 hours aged, and I and J of 1200 hours aged sample. Aging temperature 820 °C.*

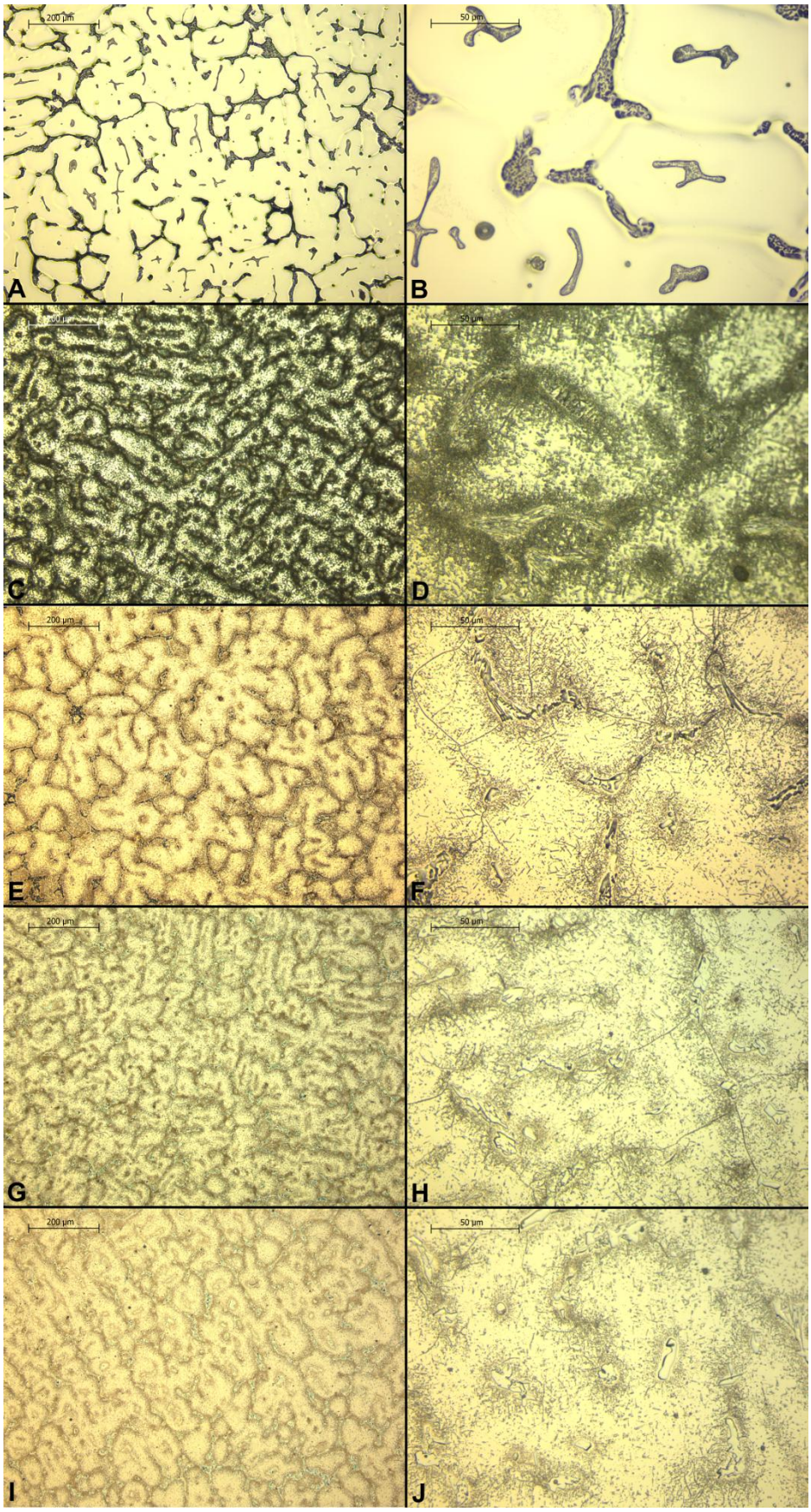

Figure 6.4. *Optical microscopy images of the steel HH (b), where A and B are of as-cast sample, C and D of 100 hours aged, E and F of 300 hours aged, G and H of 600 hours aged, and I and J of 1200 hours aged sample. Aging temperature 820 °C.*

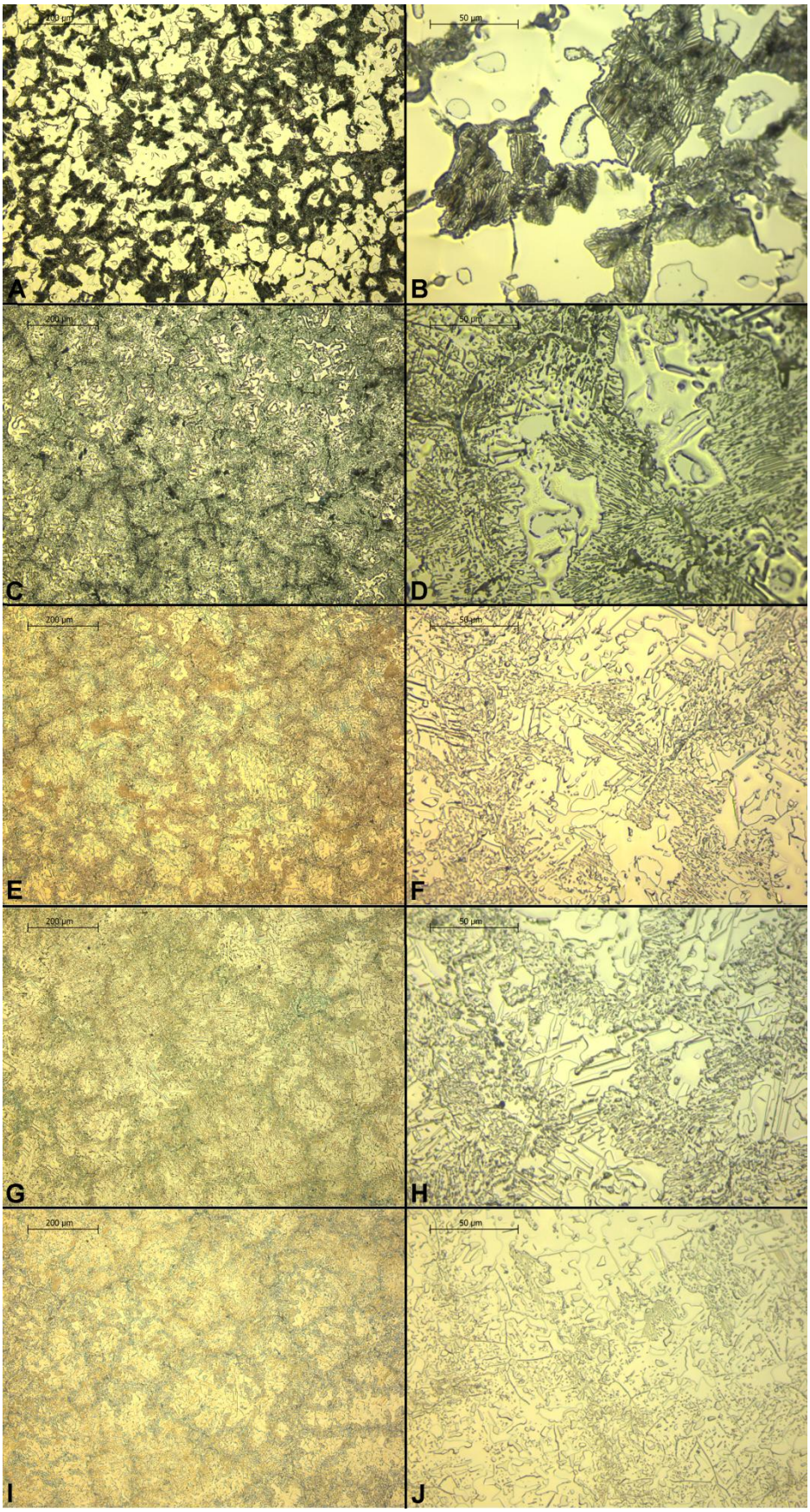

Figure 6.5. *Optical microscopy images of the steel HD, where A and B are of as-cast sample, C and D of 100 hours aged, E and F of 300 hours aged, G and H of 600 hours aged, and I and J of 1200 hours aged sample. Aging temperature 820 °C.*

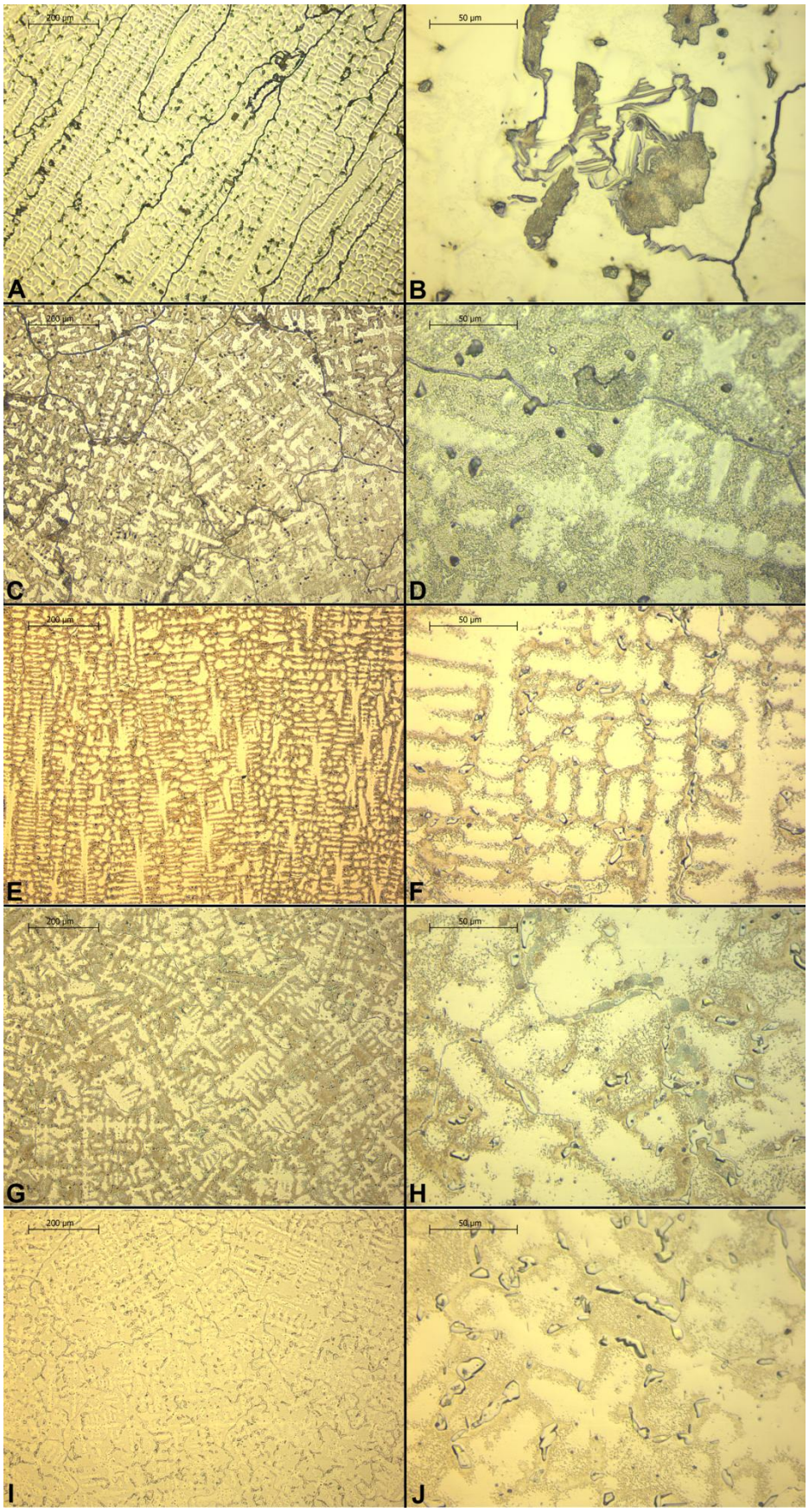

Figure 6.6. *Optical microscopy images of the steel HI, where A and B are of as-cast sample, C and D of 100 hours aged, E and F of 300 hours aged, G and H of 600 hours aged, and I and J of 1200 hours aged sample. Aging temperature 820 °C.*

Images taken from the samples, which were electrolytically etched with sodium hydroxide are presented in Figures 6.7 - 6.10. Etching with sodium hydroxide was done to reveal the sigma-phase precipitates. Sigma-phase was identified from each studied steel grade in 100 hours and 1200 hours aged conditions. The optical microscopy images are presented in the following order (see Table 6.2).

Table 6.2. *Corresponding image labels and sample conditions on the samples electrolytically etched with sodium hydroxide.*

Label on the image	Sample condition
A, B	as-cast
C, D	aged for 100 hours
E, F	aged for 1200 hours

Images were taken using different magnifications. The images shown on the left side of the figures were taken using objective magnification of 10x, the ones on the right side using objective magnification of 50x. There is a scale bar in every image to show the true magnification.

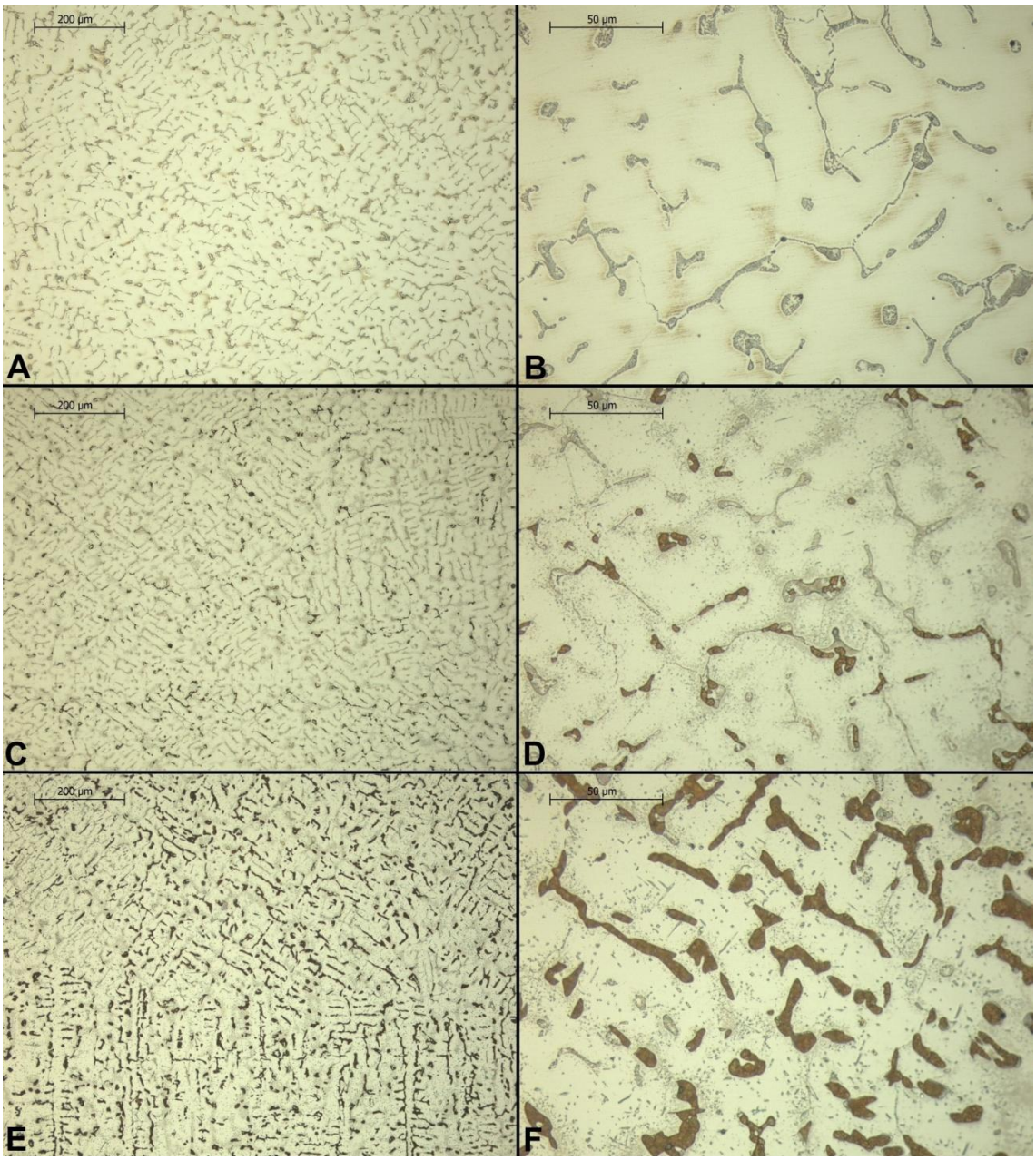

Figure 6.7. *Optical microscopy images of the steel HH (a), where A and B are of as-cast sample, C and D of 100 hours aged, and E and F of 1200 hours aged sample. Aging temperature 820 °C. Samples were etched with sodium hydroxide, which dyes the sigma-phase with brown colour.*

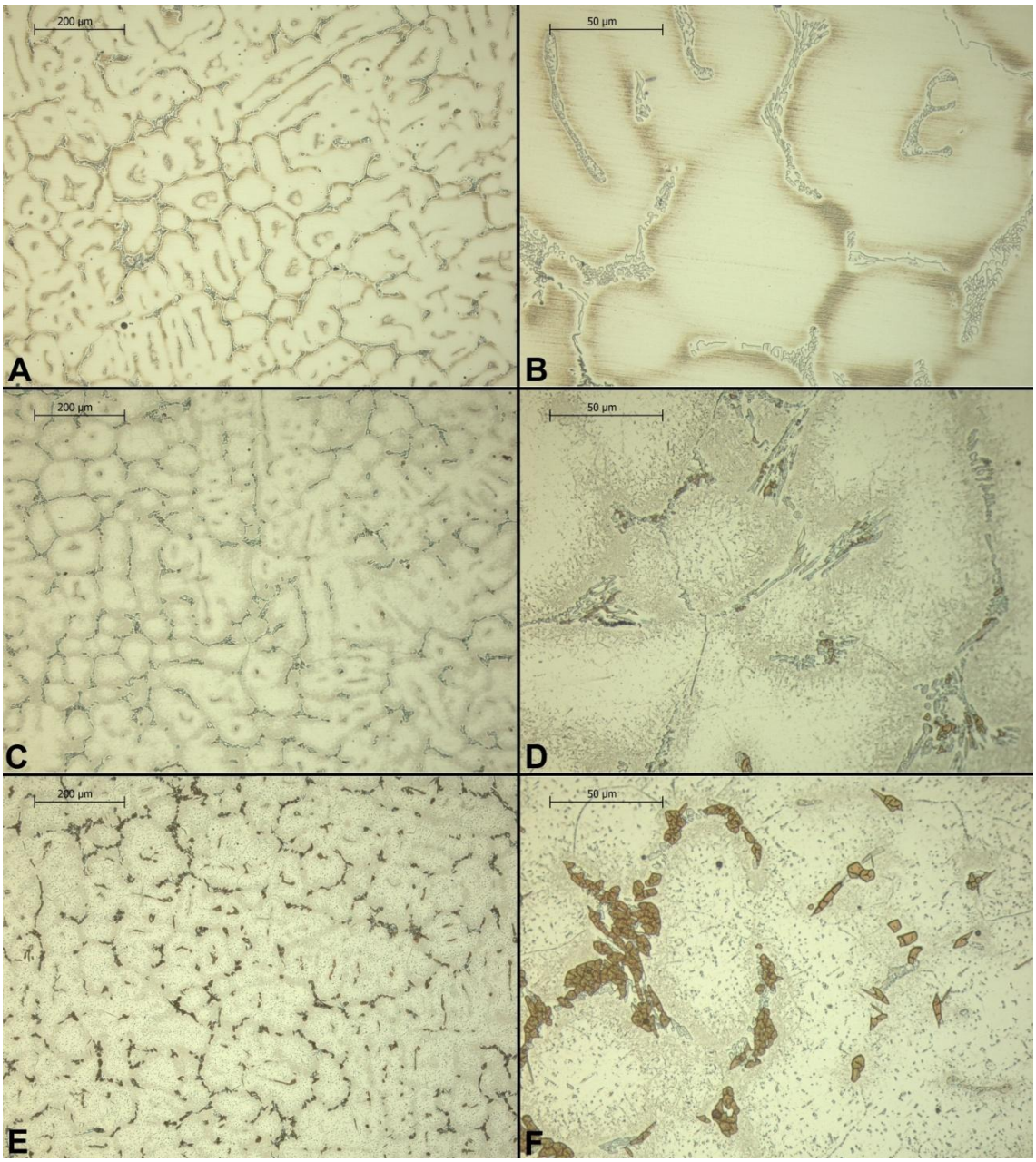

Figure 6.8. *Optical microscopy images of the steel HH (b), where A and B are of as-cast sample, C and D of 100 hours aged, and E and F of 1200 hours aged sample. Aging temperature 820 °C. Samples were etched with sodium hydroxide, which dyes the sigma-phase with brown colour.*

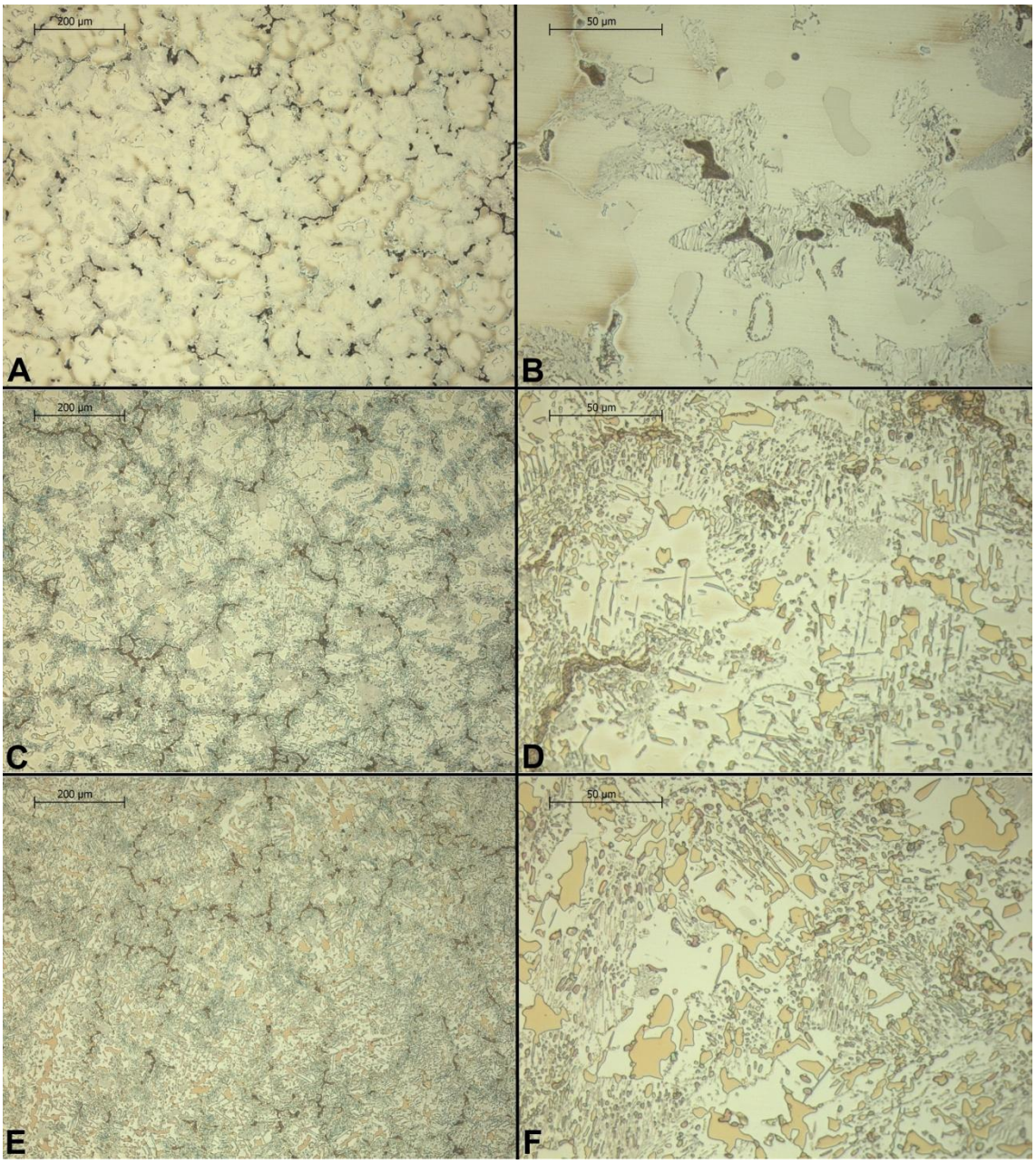

Figure 6.9. *Optical microscopy images of the steel HD, where A and B are of as-cast sample, C and D of 100 hours aged, and E and F of 1200 hours aged sample. Aging temperature 820 °C. Samples were etched with sodium hydroxide, which dyes the sigma-phase with brown colour. Here the sigma-phase coloured in light orange tone.*

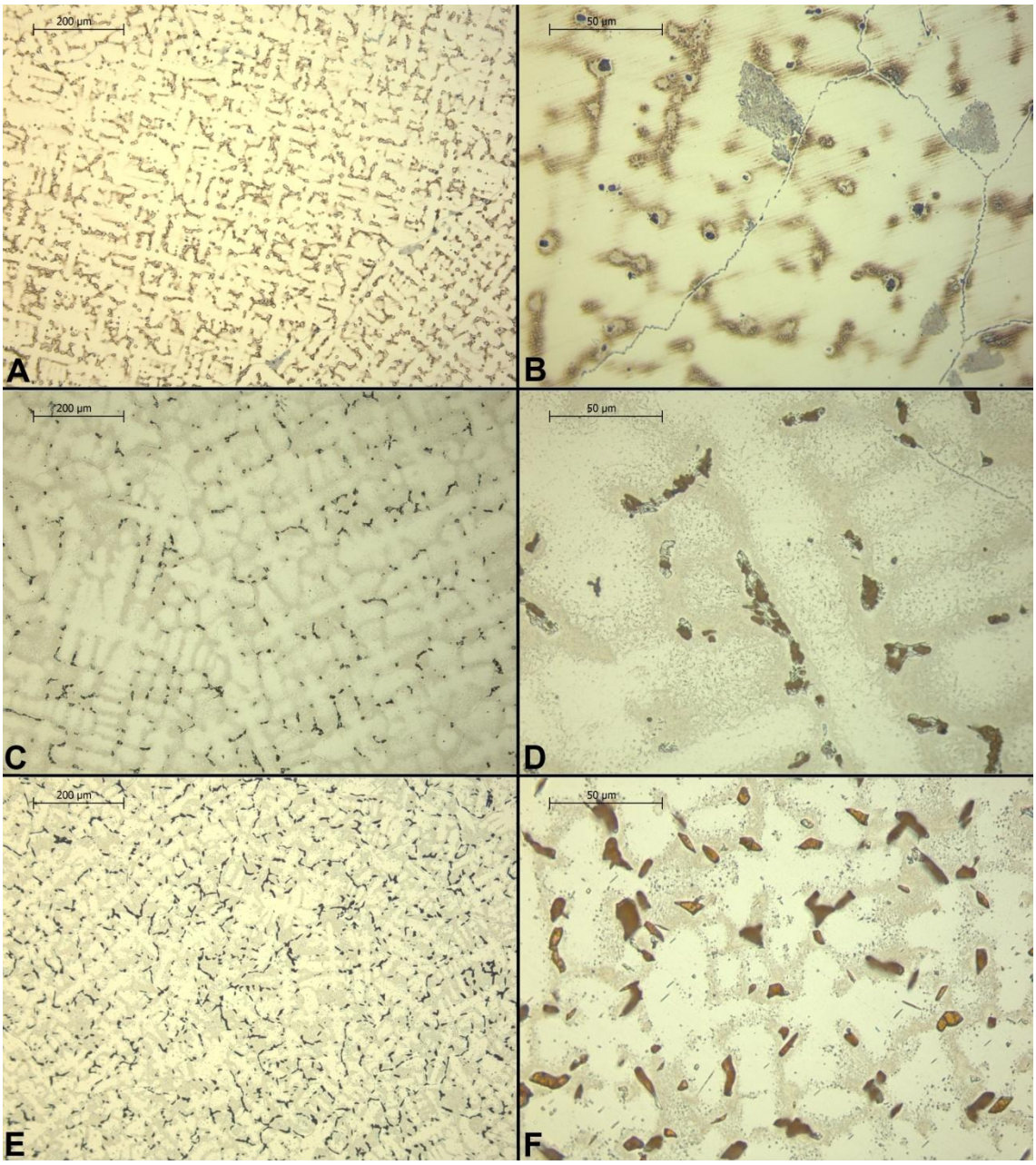

Figure 6.10. *Optical microscopy images of the steel HI, where A and B are of as-cast sample, C and D of 100 hours aged, and E and F of 1200 hours aged sample. Aging temperature 820 °C. Samples were etched with sodium hydroxide, which dyes the sigma-phase with brown colour.*

6.3.2 SEM + EDS studies

SEM images were obtained from samples electrolytically etched with oxalic acid. As-cast and 1200 hours aged samples were studied on each steel grade. Detector for either backscattered electrons (BSE) or secondary electrons (SE) was used. The detector type was chosen to obtain as much information as possible from the formed SEM image. From the following SEM images the same conclusions could be drawn as from the optical microscopy images. The microstructures of the studied grades changed drastically as a result of aging treatment at 820 °C.

Figures 6.11 - 6.18 show the obtained SEM images. Each figure is followed by a table presenting the results of the EDS analyses taken from the different phases of the studied samples (see Table 6.3 - 6.10). The compositions are given in weight percents. General analyses were calculated as an average of four individual areal analyses collected from all over the sample at a lower magnification. In reviewing the results of EDS analyses, it should be taken into account that the quantitative analysis of carbon is not accurate. However, it can be suggestive and it must be included in the studies since carbon is an element of high importance in steel structures.

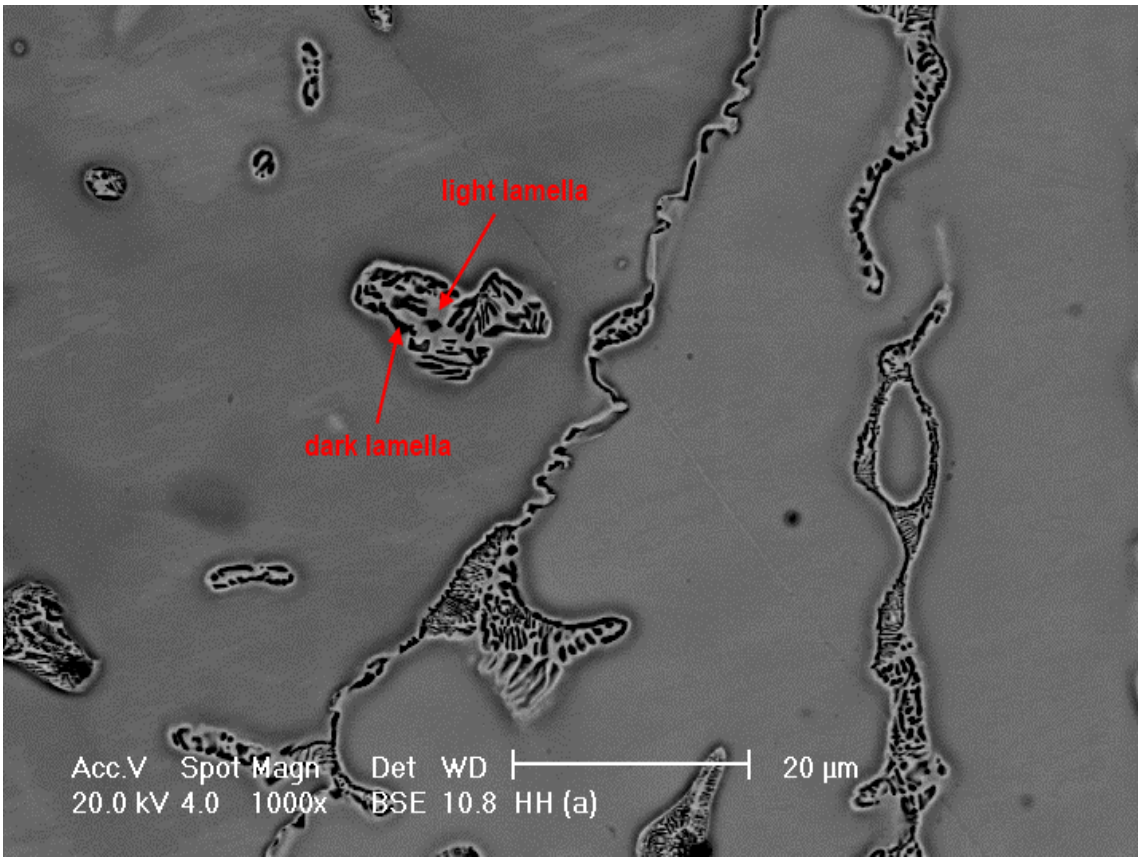

Figure 6.11. *SEM BSE image of the as-cast steel HH (a). Original magnification 1000x.*

Table 6.3. *EDS analysis of different phases in the as-cast steel HH (a). Results in wt%.*

HH (a)		C	Si	Mo	Cr	Mn	Fe	Ni
as cast	gen. analysis	3.5	1.2	0.3	24.4	1.4	56.8	12.4
	matrix phase	3.2	1.1	0.2	24.0	1.4	57.0	13.0
	light lamella	3.3	1.7	0.3	19.2	1.6	61.6	12.3
	dark lamella	1.3	0.9	0.3	26.6	1.6	58.6	10.7

Figure 6.11 shows the structure of the austenitic matrix of as-cast steel HH (a) with lamellar phase areas. No reliable EDS analysis of the dark lamellae could be obtained in the as-cast steel HH (a). Most likely it was due to the dissolution of the carbide particles as a result of electrolytical etching with oxalic acid. The reasons are discussed in more detail in Chapter 7.3.2.

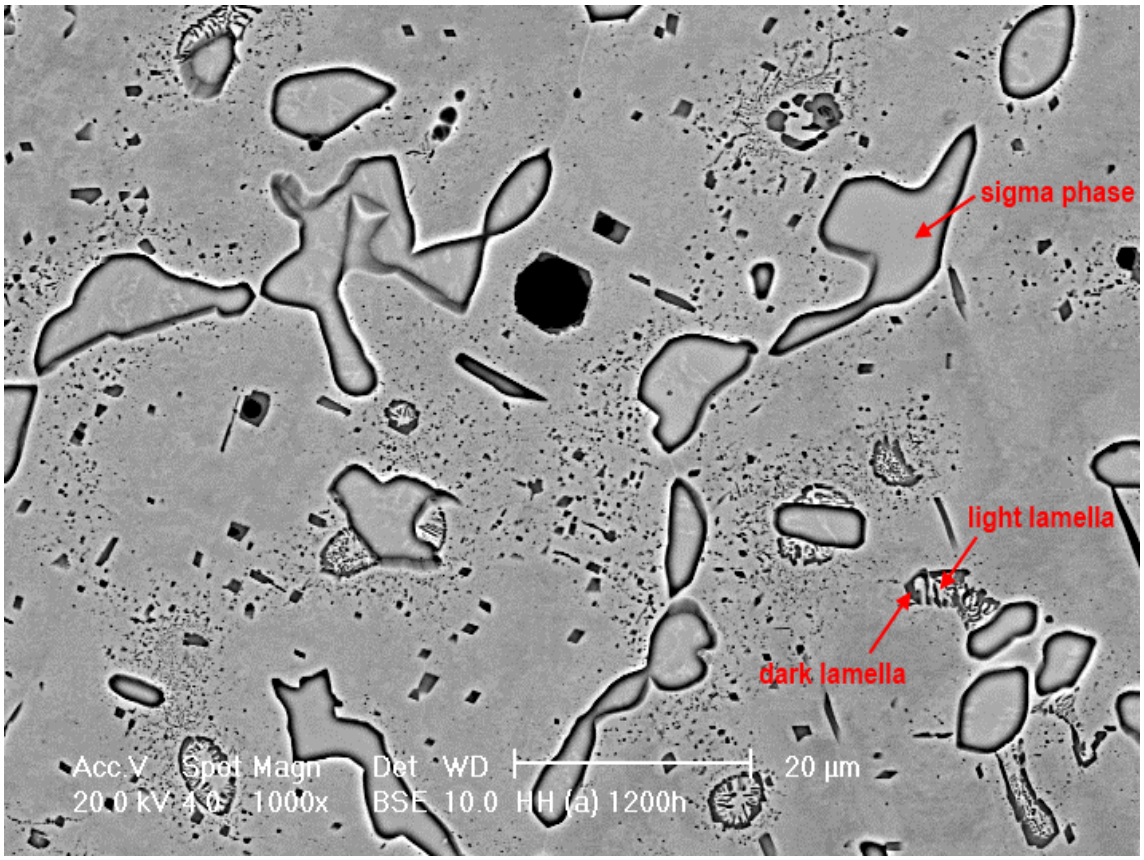

Figure 6.12. *SEM BSE image of the 1200 hours aged steel HH (a). Aging temperature 820 °C. Original magnification 1000x.*

Table 6.4. *EDS analysis of different phases in the 1200 hours aged steel HH (a). Aging temperature 820 °C. Results in wt%.*

HH (a)		C	Si	Mo	Cr	Mn	Fe	Ni
1200h	matrix phase	3.8	1.4	0.5	21.1	1.7	58.3	13.7
	sigma-phase	3.3	2.3	1.1	38.7	1.5	46.4	6.7
	light lamella	6.4	1.2	0.7	31.9	1.4	48.1	10.3
	dark lamella	8.0	0.3	1.7	65.3	0.8	19.9	4.0

The complex structure containing several different precipitates of the 1200 hours aged HH (a) is shown in Figure 6.12. Lamellar phase areas have disappeared for the most part. Sigma-phase has precipitated homogenously throughout the structure. Carbide lamellae have dissolved in the matrix and small carbide particles have reprecipitated. The size of the precipitates with regular geometric shapes did not enable the EDS analysis.

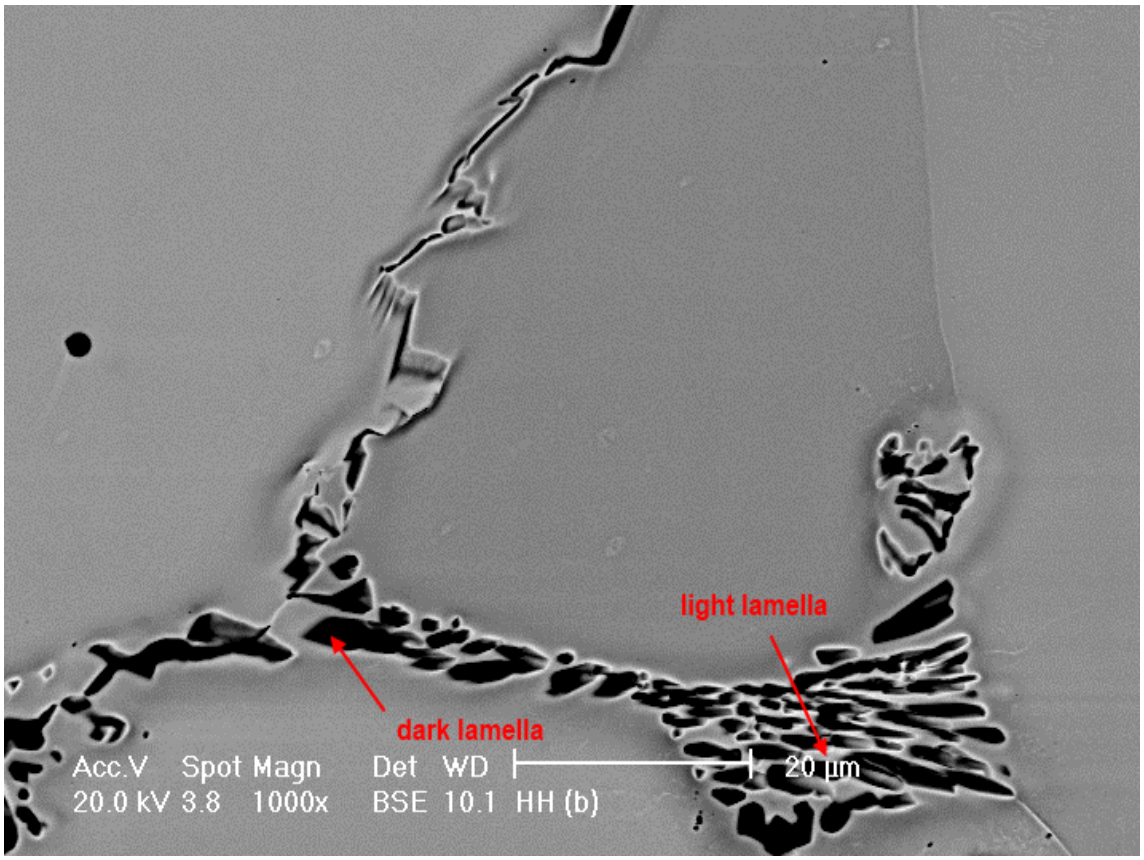

Figure 6.13. *SEM BSE image of the as-cast steel HH (b). Original magnification 1000x.*

Table 6.5. *EDS analysis of different phases in the as-cast steel HH (b). Results in wt%.*

HH (b)		C	Si	Mo	Cr	Mn	Fe	Ni
as cast	gen.analysis	5.0	1.4	0.4	23.2	1.0	56.4	11.6
	matrix phase	3.3	1.4	0.2	23.9	1.0	58.1	12.1
	light lamella	5.8	2.5	1.1	15.6	1.1	67.0	7.0
	dark lamella	14.0	1.4	0.3	18.7	1.3	56.0	8.3

As can be seen in Figure 6.13, the grain size of the steel HH (b) is significantly larger than that of the steel HH (a). Otherwise the structures are quite similar, austenitic matrix with lamellar phase areas.

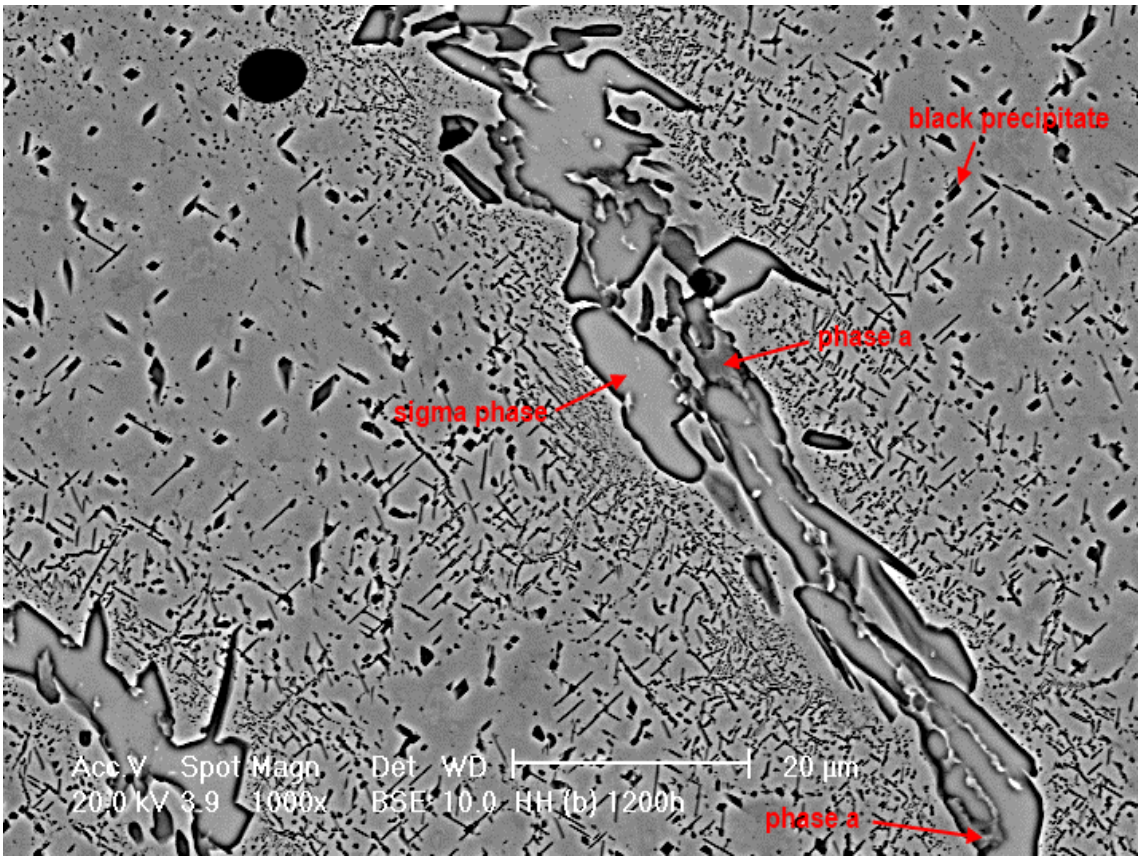

Figure 6.14. *SEM BSE image of the 1200 hours aged steel HH (b). Aging temperature 820 °C. Original magnification 1000x.*

Table 6.6. *EDS analysis of different phases in the 1200 hours aged steel HH (b). Aging temperature 820 °C. Results in wt%.*

HH (b)		C	Si	Mo	Cr	Mn	Fe	Ni
1200h	matrix phase	4.1	1.4	0.4	23.4	1.2	57.1	12.5
	sigma-phase	3.5	2.4	1.8	37.9	1.1	47.0	6.2
	phase a	10.3	0.2	1.6	70.1	0.5	15.1	2.2
	black precipitates	5.8	0.5	1.1	41.3	1.1	42.1	8.0

Figure 6.14 shows the microstructure of the 1200 hours aged steel HH (b). Lamellar phase areas have disappeared. Carbide lamellae have dissolved in the matrix and smaller carbide particles have reprecipitated. The needle-like precipitates are most likely sigma-phase precipitates, which have quite homogenously distributed in the structure. Chromium-rich phase a has precipitated close to larger sigma-phase precipitates.

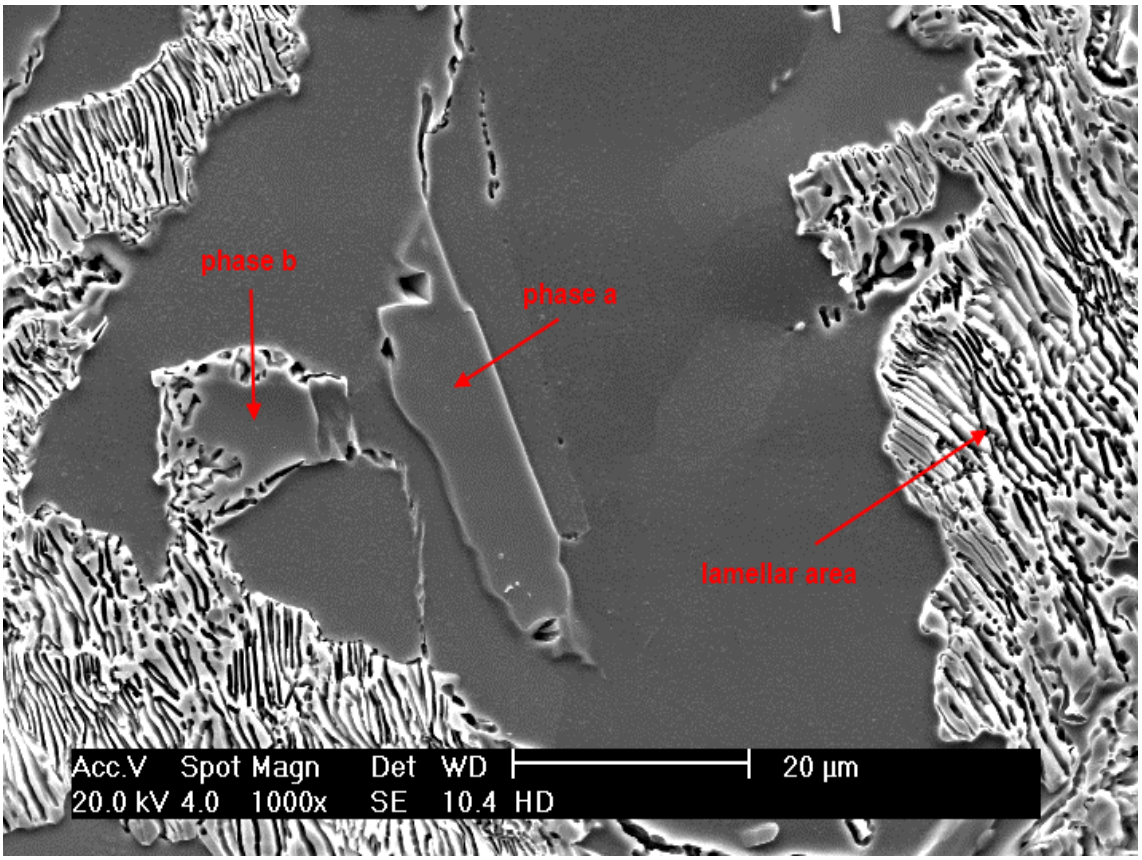

Figure 6.15. *SEM SE image of the as-cast steel HD. Original magnification 1000x.*

Table 6.7. *EDS analysis of different phases in the as-cast steel HD. Results in wt%.*

HD		C	Si	Mo	Cr	Mn	Fe	Ni
as cast	matrix phase	3.3	3.1	0.4	25.1	1.1	60.5	6.7
	phase a ("clean")	3.7	3.5	0.5	25.2	0.9	61.3	5.0
	phase b ("edged")	3.1	4.0	0.6	21.5	0.9	65.2	4.7
	lamellar area	3.7	2.9	0.5	23.2	1.3	61.4	7.1

Massive amount of lamellar phase areas in as-cast steel HD can be seen in Figure 6.15. The compositional EDS analyses were carried out on phase a (“clean”) and phase b (“edged”) individually, because these phases showed different structures. Phase a (“clean”) had no lamellar constituent surrounding it. On the other hand, phase b (“edged”) was surrounded by lamellar constituent. Phase b (“edged”) had lower chromium content most likely because the chromium carbide lamellae on the boundary had consumed some chromium and left the inside phase somewhat chromium depleted.

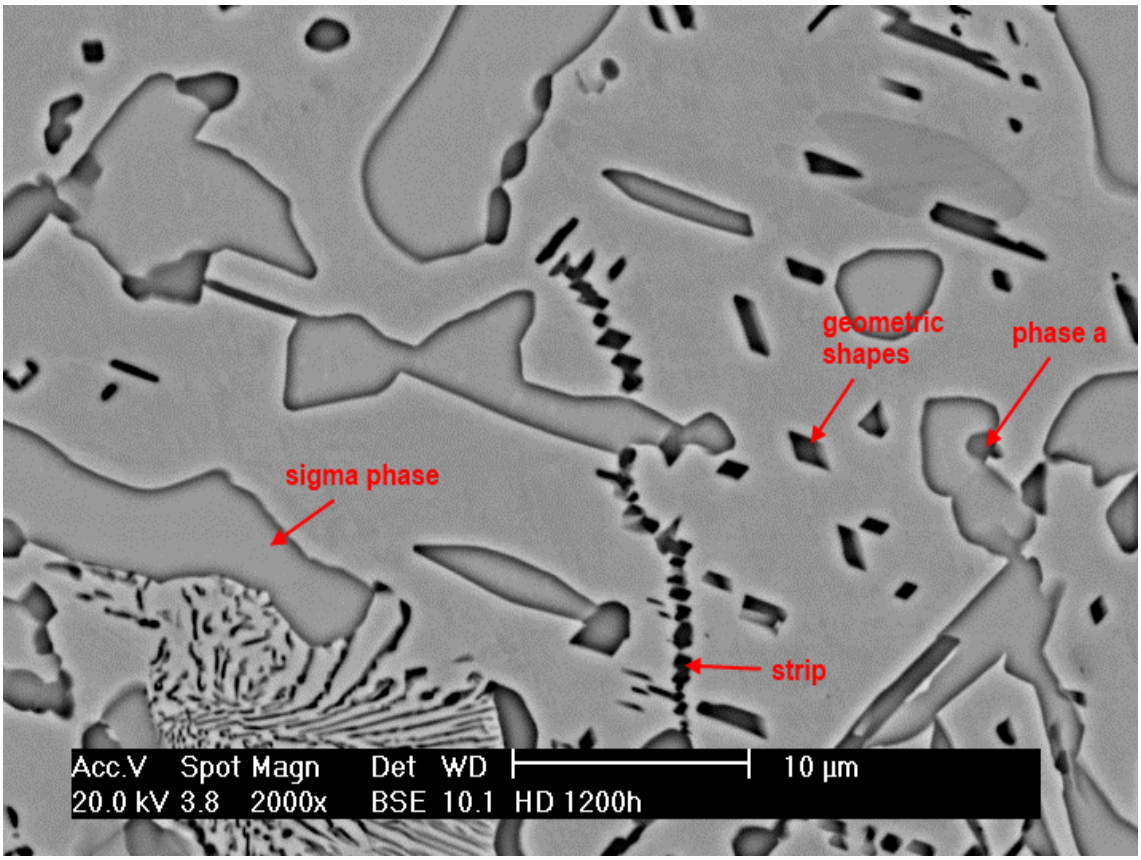

Figure 6.16. *SEM BSE image of the 1200 hours aged steel HD. Aging temperature 820 °C. Original magnification 2000x.*

Table 6.8. *EDS analysis of different phases in the 1200 hours aged steel HD. Aging temperature 820 °C. Results in wt%.*

HD		C	Si	Mo	Cr	Mn	Fe	Ni
1200h	matrix phase	3.1	2.8	0.3	19.6	1.1	67.9	5.2
	sigma-phase	2.7	4.1	0.9	32.6	1.1	55.1	3.5
	geometric shapes	2.1	1.1	0.3	30.1	1.2	59.5	5.9
	strip	1.2	0.6	0.9	58.8	1.1	33.8	3.5
	phase a	4.1	2.0	0.5	21.4	1.2	64.7	6.1

The microstructure of the 1200 hours aged steel HD is shown in Figure 6.16. Most of the lamellar phase areas have disappeared. There is no similar distribution of tiny carbide particles in the 1200 hours aged steel HD as in the 1200 hours aged steels HH (a) and HH (b). Sigma-phase has precipitated homogenously throughout the structure.

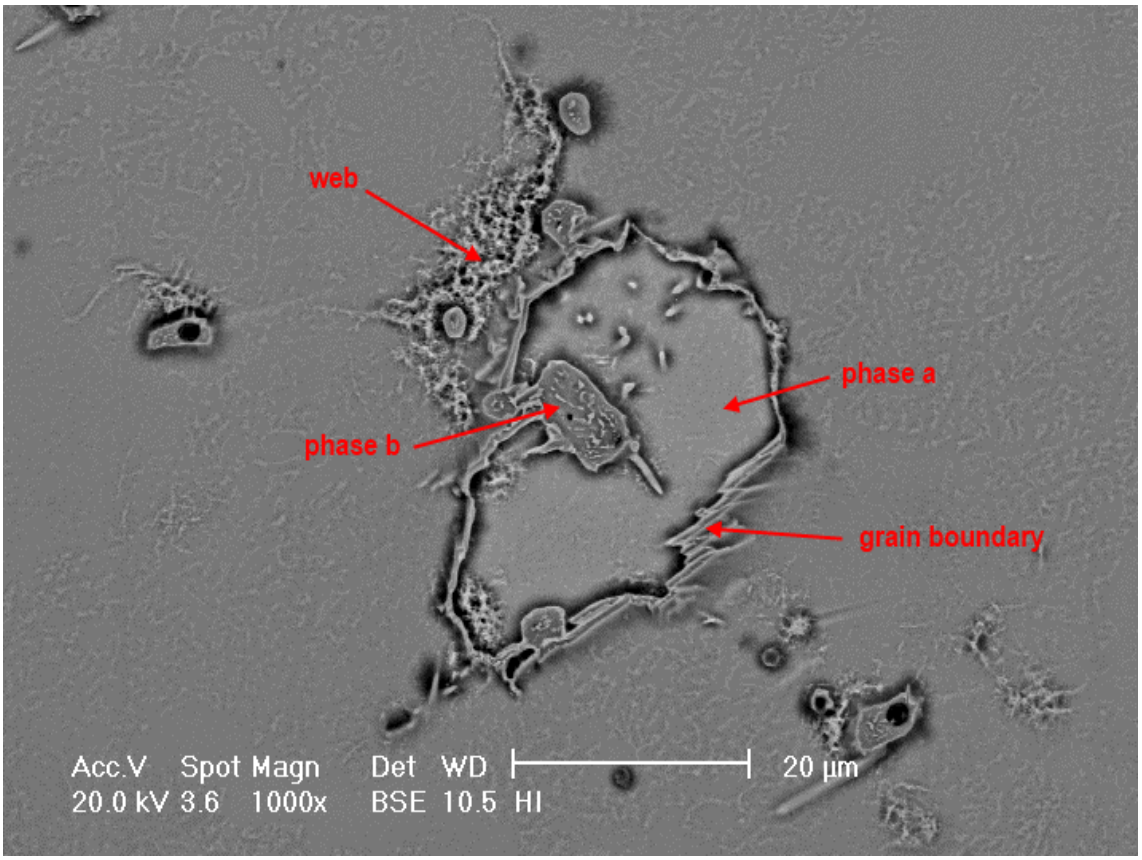

Figure 6.17. *SEM BSE image of the as-cast steel HI. Original magnification 1000x.*

Table 6.9. *EDS analysis of different phases in the as-cast steel HI. Results in wt%.*

HI		C	Si	Mo	Cr	Mn	Fe	Ni
as cast	gen.analysis	2.9	1.1	0.3	26.5	1.3	51.1	16.5
	matrix phase	2.1	1.0	0.4	25.4	1.3	52.8	16.6
	phase a	3.1	1.2	0.3	27.6	1.4	49.8	16.3
	phase b	10.9	0.5	1.2	53.8	0.7	27.1	5.5
	web	5.1	1.1	0.3	31.9	1.5	45.2	14.6
	grain boundary	9.7	0.9	0.3	37.8	1.2	37.6	12.2

The completely austenitic matrix of the as-cast steel HI is shown in Figure 6.17. Carbide precipitates are located near grain boundaries and in the matrix. There is no continuous network of carbides.

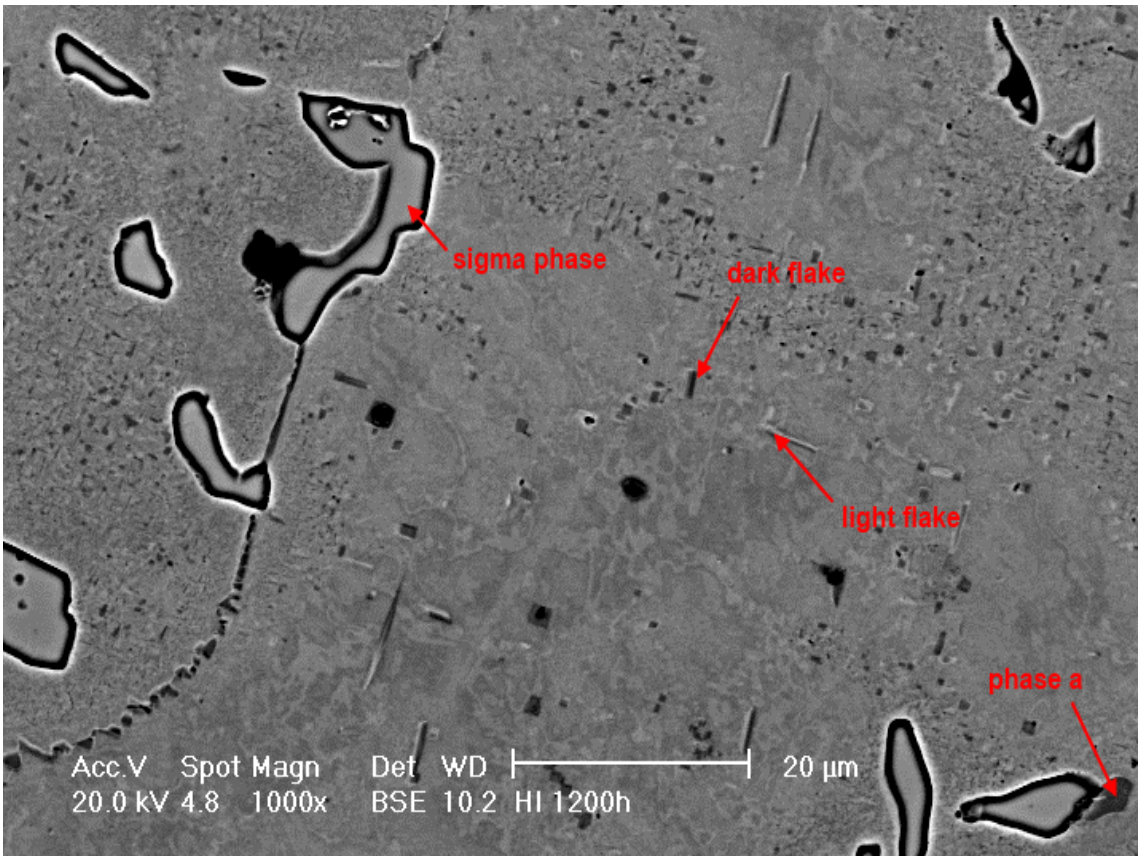

Figure 6.18. *SEM BSE image of the 1200 hours aged steel HI. Aging temperature 820 °C. Original magnification 1000x.*

Table 6.10. *EDS analysis of different phases in the 1200 hours aged steel HI. Aging temperature 820 °C. Results in wt%.*

HI		C	Si	Mo	Cr	Mn	Fe	Ni
1200h	matrix phase	3.6	1.2	0.4	22.6	1.7	53.6	16.9
	sigma-phase	3.2	2.0	0.8	41.5	1.4	42.8	8.4
	phase a	8.5	0.2	1.0	74.3	0.5	12.6	3.0
	dark flake	8.2	0.7	0.8	55.7	1.0	25.3	8.4
	light flake	7.2	0.9	0.6	31.6	1.3	44.7	13.8

Figure 6.18 shows the microstructure of the 1200 hours aged steel HI with the austenitic matrix and numerous precipitates. As in steel HH (b) chromium-rich phase a has precipitated close to the sigma-phase. Grain boundary carbides have dissolved and reprecipitated.

7 DISCUSSION

The findings of the tests presented in Chapter 5 are discussed in the following. Results of each test type are discussed separately. Altogether the experimental part of the thesis was successful and the results were in line with the presumptions prior to the tests. Microstructural characterisation produced some unexpected results concerning the changes in the microstructures due to aging.

7.1 Impact toughness

In general the impact toughness test results were consistent with the prior studies and the expectations of the author. Figure 6.1 on page 36 shows the impact toughness values of each grade as a function of the aging time. Original impact toughness values of as-cast samples had high scatter depending on the steel grade. Completely austenitic steel HI had the highest impact toughness value of nearly 35 J, whereas the as-cast two-phase steel HD was the most brittle as-cast material of the set. Its impact toughness was measured to be only slightly over 10 J. Basically austenitic grades HH (a) and HH (b) showed impact toughness values between the grades HI and HD in as-cast condition. Therefore the results indicated that the ductility of the material increased with increasing austenite content. As a whole this type of behaviour is typical of stainless steels [5].

It can be seen in Figure 6.1 that the impact toughness values of each steel grade decreased as the time of aging increased. For every studied steel grade, there was a significant drop in the measured impact toughness values after only 100 hours of aging. This result was not fully expected. The decrease got smaller with increasing aging time in the 300, 600, and 1200 hours aged samples. 1200 hours aged samples showed nearly no difference in the impact toughness measurements between different steel grades.

The standard deviations of the tested impact toughness values measured for the steel grades HH (a), HH (b), HD, and HI are presented in Table 7.1. The test series consisted of three measurements per each steel grade and aging time combination. The measurements of as-cast and 100 hours aged samples were carried out with a different type of impact testing machine than the measurements on the 300, 600, and 1200 hours aged samples. This must be taken into account when the test results are interpreted.

The standard deviations of as-cast samples were much higher than those of aged samples. It might have been due to the eventually non-uniform sample collection. Even a tiny pore in the material could have influenced the measurement results greatly by decreasing the otherwise higher impact toughness of the material. Aged samples had more uniform structures and therefore they did not have as much scatter in their measurement results.

Table 7.1. *The standard deviations of the impact toughness values of the tested steel grades.*

Standard deviation					
	As cast	100h	300h	600h	1200h
HH (a)	13.2	5.8	0.4	0.6	0.4
HH (b)	9.0	0.5	0.3	0.5	0.1
HD	11.4	0.3	0.2	0.2	0.2
HI	24.1	1.9	1.3	0.7	0.6

On the basis of the results the microstructures of each steel grade changed substantially after 100 hours of aging. The changes in microstructure embrittled the material. As stated earlier in Chapter 3.2.1 this embrittlement could have resulted either from the formation of the sigma-phase or from the dispersion of different types of carbides.

7.2 Hardness

Hardness measurements in Figure 6.2 on page 37 showed a significant dependency of the hardness on the steel grade. The two-phase ferritic-austenitic HD exceeded all other grades in hardness by having almost double hardness (over 300 HV3 in each condition) as compared to the other grades. HH (a), HH (b), and HI all showed nearly similar results, hardness values close to 200 HV3. The superiority of HD in hardness resulted most likely from its two-phase ferritic-austenitic structure and its high carbide content (see microscopy images in Chapter 6.3).

Each grade had a slight increase in hardness with increasing aging time. This increase was likely due to the precipitation of hard phases, such as the sigma-phase. Also the fine dispersion of the carbide particles could have resulted in the increase of the overall hardness. The microstructural changes are discussed in Chapter 7.3.

Table 7.2. *The standard deviations of the hardness values of the tested steel grades.*

Standard deviation					
	As cast	100h	300h	600h	1200h
HH (a)	10.2	5.1	6.3	5.9	5.7
HH (b)	6.0	9.7	16.0	6.0	9.4
HD	14.7	11.6	18.4	18.1	13.8
HI	5.8	6.7	5.4	3.6	10.7

The standard deviations of the hardness values of the tested steel grades HH (a), HH (b), HD, and HI are presented in Table 7.2. The test series consisted of ten measurements per each steel grade and aging time combination. There was no relation between the changes in standard deviations and the aging times. However, the deviations of the grade HD were without exception higher than those of other grades. This resulted from

the differences in the microstructures between the two-phase ferritic-austenitic grade HD and the austenitic grades HH (a), HH (b), and HI.

In the measurements the pyramid-shaped hardness indenter was pressed against the surface of the test material. The measurement locations were chosen so that the resulting indentations covered more than a single phase. Examples of indentations are shown in Figure 7.1. As stated earlier, the reason behind the greater standard deviations in the hardness of the steel HD was in its microstructure, which differed greatly from the others. The microstructure of HD consisted of two phases. Though the indentation covered both of these two phases, the volume fractions of the phases hit by the indentation could have varied greatly from one indentation to another. Therefore a single hardness measurement from HD reflected the hardness of that single spot and there were great differences in the individual measurement results. The same reasons applied to the great standard deviations of other grades as well, even though the issue was not that as significant as in the case of steel HD.

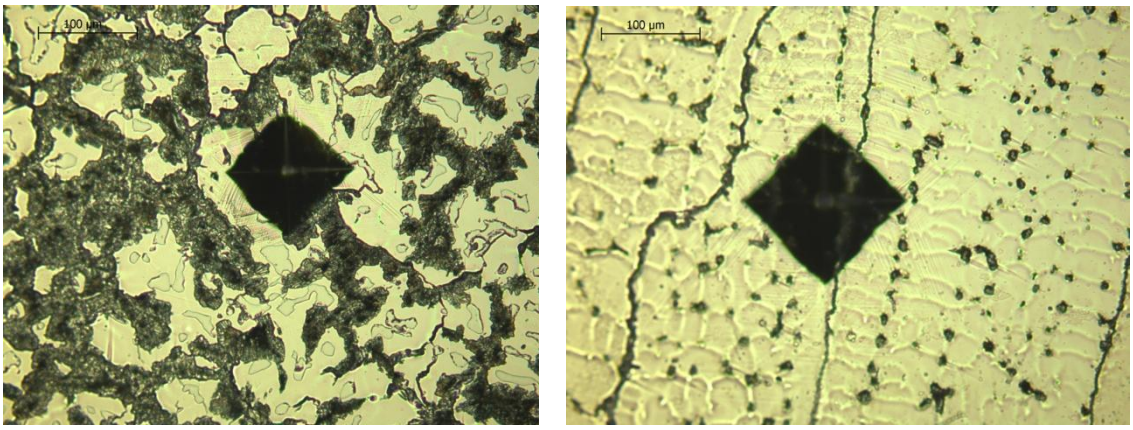

Figure 7.1. *The hardness measurement indentations on the as-cast steel HD (left) and on the as-cast steel HI (right). Objective magnification 20x.*

7.3 Microstructural characterisation

Microstructural characterisation was an extensive part of the experimental studies. The studied microstructures proved to be more complex than expected. Especially SEM + EDS studies revealed highly complex microstructures and plenty of different types of precipitates.

7.3.1 Optical microscopy

Samples electrolytically etched with oxalic acid and samples electrolytically etched with sodium hydroxide showed the changes in microstructure in a different way. Electrolytical etching with oxalic acid revealed the microstructure and the different phases present, but there was no significant dyeing of one single phase. On the contrary, etching the aged samples with sodium hydroxide dyed one phase that clearly differed from the other

phases in etched samples. In steels HH (a), HH (b), and HI this phase was coloured brown, and in steel HD in light orange tone.

Another noteworthy observation on the images was the differences between different grades of steel. HH (a), HH (b), and HI had rather similar microstructures, especially after 1200 hours of aging at 820 °C. The microstructure of HD was noticeably different. According to ASM Specialty Handbook of Stainless Steels the microstructures of HH (a), HH (b), and HI are basically austenitic, whereas the microstructure of HD is a two-phase ferritic-austenitic [32]. The as-cast HD showed a microstructure with plenty of lamellar phase-mixture. Sodium hydroxide etched as-cast HD sample showed also darker coloured phase in the middle of the lamellar phase areas. According to etching guides (for example see Ref. 32) ferrite is coloured tan when sodium hydroxide is used as an etchant. The same sources state that when oxalic acid is used, ferrite is unattacked. These matters kept in mind, the darker coloured phase in the middle of the lamellar phases in HD visible in Figure 6.9 could have actually been ferrite, since the same type of phase did not stand out in Figure 6.5.

The same type of lamellar phase as in HD precipitated near grain boundaries in grade HI. Earlier studies of microstructures of cast stainless steels indicate that this lamellar phase consists of alternating plates of austenite and carbide [32]. The plates of austenite appeared light coloured in the images, whereas the carbide plates appeared dark coloured. Also the dark coloured carbide networks in HH (a) and HH (b) were likely to consist of lamellar carbides and austenite.

Etching guides suggest that using sodium hydroxide as an etchant leads to staining the sigma-phase brown in austenitic grades [36]. HH (a), HH (b), and HI had brown coloured phase in both 100 hours and 1200 hours aged samples. On this basis, it was concluded that those brown coloured phases were sigma-phase precipitates. The SEM + EDS studies supported this conclusion. Sigma-phase had also precipitated in HD, but it showed a light orange colouring.

An important conclusion was drawn from the optical microscopy studies. All grades had sigma-phase present in their microstructures even after 100 hours aging at 820 °C. The results of the studies on samples etched with sodium hydroxide verified this. The amount of sigma-phase increased with increasing hours of aging. 1200 hours aged samples showed more sigma-phase than 100 hours aged ones. This result correlated well with the results from the impact toughness tests. Since even small amounts of sigma-phase can result in major loss in impact toughness, the results based on this study supported the argument of sigma-phase being the embrittling factor in the studied steels.

7.3.2 SEM + EDS studies

The results of SEM + EDS studies supported the results of optical microscopy studies. The microstructures changed drastically during aging treatments. Rather simple structures of as-cast samples turned into highly complex structures with several different precipitates.

A major problem in SEM + EDS studies turned out to be the used etchant. The studies were carried out on samples, which were etched with oxalic acid. The etchant proved to be a good choice for revealing the overall microstructure including the sigma-phase. The disadvantage in using oxalic acid was the dissolution of carbides as a result of etching. Considering this, the cavities observed in SEM studies could rather easily be interpreted as previous positions of carbide particles.

In addition to the dissolved carbides, there was another problem in the SEM + EDS studies. Most of the newly formed precipitates were too small in size in order to obtain any reliable analysis. This was a problem especially with the 1200 hours aged samples. Even though the precipitate would have been large enough, the analysis information still would have come from the surrounding phases as well. This is due to the pear-shaped geometry of the detection volume. In practice this means that the analysis information is collected not only from the surface but also from a certain depth of the samples. The information coming below the surface is collected from a bigger volume area than what the electron beam covers on the sample surface. Despite this fact, the SEM studies gave some important information on the small precipitates. Most of them were cavities, indicating that there had been small carbide precipitates present prior to etching.

The EDS analyses of the matrix phases of HH (a), HH (b), and HI indicated an austenitic structure with rather high amounts of nickel, as suspected. Only minor differences in the compositions of the matrix phase between as-cast and 1200 hours aged samples existed. The matrix phase of HD differed from that of the basically austenitic steel grades. HD had only 6.7 wt% nickel content in the matrix phase in the as-cast sample compared to the nickel content of 16.6 wt% in the matrix phase of the as-cast sample HI.

Sigma-phase was identified in all studied samples based on the findings of optical microscopy and SEM + EDS studies. Depending on the studied steel grade, the sigma-phase had slightly differing compositions. As presented earlier in Chapter 3, the composition of sigma-phase varies with different steel grades. The results of SEM + EDS studies suggested that the sigma-phase compositions in austenitic grades HH (a), HH (b), and HI were richer in nickel and poorer in silicon than the sigma-phase composition in the two-phase ferritic austenitic grade HD.

Sigma-phase had formed in the studied steel grades in differently shaped precipitates. Large sigma-phase particles had precipitated in each grade. Grade HH (b) had also a significant amount of needle-like sigma-phase platelets. Babakr et al. [37] found in their study the same type of sigma-phase precipitates in grade HK-40 steel after approximately six months of aging at 850 °C. As this study, their study verified the precipitation of secondary carbides as well.

Other findings of SEM + EDS studies consisted of different types of lamellar structures in as-cast samples. The grain size of HH (b) was clearly bigger than the grain size of HH (a). Therefore the sizes of the lamellae were also different. The small size of single dark lamella made it more difficult to receive reliable data on EDS of the dark lamellae of HH (a). This was the case in analysing the lamellae of the grade HD as well.

In addition the problem was formed by the dissolved carbides. No reliable EDS analysis of dark lamellae was obtained since most of these spots were hollow.

Completely austenitic HI showed carbide structures near grain boundaries and as separate islands in the matrix in the as-cast sample. Phase b shown in Figure 6.17 was large enough to get a proper EDS analysis. The results in Table 6.9 show that both phase b and grain boundary area had increased carbon and chromium contents as compared to the matrix. This result indicates that these structures were chromium carbides. Such clear results were not received from any other grades in as-cast samples.

1200 hours aged samples showed very small precipitates in the SEM studies. On the basis of the theoretical part and earlier studies the findings suggest that the carbide networks of the as-cast samples had been scattered and the carbides had partly been dissolved and reprecipitated all over the matrix phase [32]. According to the EDS results, nearly all of the analyses from the black precipitates and dark coloured phases showed high chromium contents.

Since grade HD is slightly alloyed with nitrogen there was a possibility that also nitrides had precipitated as a result of the aging at 820 ˚C. This could not be verified in the SEM studies due to the small size of the precipitates. However, the precipitates in Figure 6.16 had a geometrical shape, which supports this presumption.

8 CONCLUSIONS

The microstructural and property changes in heat-resistant cast stainless steels after aging at 820 ˚C were studied. Impact toughness tests and hardness measurements were carried out on austenitic grades HH (a), HH (b), and HI, and on ferritic-austenitic grade HD. Extensive microstructural characterisation included optical microscopy and SEM + EDS studies.

The results of mechanical testing were mostly in line with expectations. Impact toughness test results showed the embrittlement of each studied steel grade. The embrittlement phenomenon was strongest after 100 hours of aging. This was not expected. Hardness measurement results verified the predictions of increased hardness values after aging. Each studied steel grade had a clear increase in their hardness values. The hardness values of two-phase steel grade HD were significantly higher than those of the austenitic steel grades. Impact toughness test results did not show such clear differences, even though grade HD had the lowest ductility throughout the test.

Microstructural characterisation revealed highly complex microstructures in all studied steel grades. Samples aged at 820 ˚C for 1200 hours showed a large number of different precipitates. Sigma-phase was identified in all studied steel grades already after 100 hours aging. 1200 hours aged samples showed fairly large sigma-phase precipitates which were homogenously distributed. It was somewhat surprising that the sigma-phase had precipitated during the relatively short aging time of 100 hours also in the completely austenitic grade HI. The results of optical microscopy indicated signs of redistribution of carbides due to aging. As-cast samples showed carbide clusters which were almost fully dispersed in the 1200 hours aged samples. The use of oxalic acid as an etchant should be avoided in further studies in order to obtain more reliable results of carbide analysis in SEM + EDS studies.

The findings of microstructural characterisation supported the results of mechanical testing. Altogether, the results of the experimental part correlated well with the theoretical background. The embrittlement phenomena, which were observed in this study most likely resulted from the combination of the formation of sigma-phase and the dispersion of fine carbide particles.

9 RECOMMENDATIONS FOR FURTHER STUDIES

The results of the impact toughness tests were not completely in line with expectations. There was a significant drop in the ductility of each grade after only 100 hours of aging. In practice this means that 100 hours of aging was enough to change the microstructures in such a way that the materials became more brittle. It would be important to study the microstructures of the 100 hours aged samples in more detail with SEM and EDS analyses. These studies should be carried out on samples etched with sodium hydroxide, as also all of the other future SEM studies, since oxalic acid proved to dissolve carbide particles.

Since sigma-phase was already found after 100 hours aging, it would be interesting to study its possible formation in shorter aging treatments. Literature references suggest that the formation of sigma-phase in austenitic stainless steels requires truly long aging times. However, in this study, the sigma-phase was found in the completely austenitic steel grade HI already after 100 hours of aging. There might be a need for studying aging times of, for example, 10, 30, and 60 hours.

In further studies, it would be worth trying to test the influence of prior homogenisation annealing on the microstructures. Annealing could provide a homogenous structure, which could eliminate the structural differences that might have influenced the results of the mechanical testing in this study. This could have a reducing influence on the standard deviations of the impact toughness test results. Most likely the prior homogenisation annealing could retard the sigma-phase formation, since there would be smaller amount of nucleation sites available for its precipitation in the microstructure.

In this study, there was a low number of test samples on each grade and condition. The amount was limited due to the tight time schedules and the large number of studied test materials. In further studies, testing with higher numbers of test samples might reduce the standard deviations of the mechanical tests and that way improve the reliability of the tests.

The methods used in microstructural characterisation did not enable carbide identification in this study. In future the use of methods suitable for carbide identification should be considered, since carbides are besides the sigma-phase a major factor causing the embrittlement of these materials.

REFERENCES

[1] Davis, J.R. (ed.) Metallurgy and Properties of Cast Stainless Steels in ASM Specialty Handbook Stainless Steels. 1st ed. (1994), pp. 66-88.

[2] ASTM Standard A781/A781M Specification for Castings, Steel and Alloy, Common Requirements for General Industrial Use. (1998).

[3] Blair, M. Specialty Steels and Heat-Resistant Alloys, Cast Stainless Steels in Metals Handbook Volume 1. 1st ed. ASM International (1990), pp. 908-929.

[4] Peckner, D., Bernstein, I.M. Handbook of Stainless Steels. McGraw-Hill Book Company (1977).

[5] Callister, W.D.J. Materials Science and Engineering, an Introduction. 6th ed. John Wiley & Sons (2003), p. 820.

[6] Kelly, J. Heat Resistant Alloys. Rolled Alloys (2005), p. 146.

[7] Sourmail, T. Stainless Steels. [WWW] Available: http://thomas-sourmail.net/stainless/index.html. [Accessed: 28-Nov-2011].

[8] Okamoto, H. Cr (Chromium) Binary Alloy Phase Diagrams. ASM Handbooks Online (1990). [WWW] Available: http://products.asminternational.org/hbk/index.jsp. [Accessed: 22-Sep-2011].

[9] Cr (Chromium) Binary Alloy Phase Diagrams. ASM Handbooks Online (1990). [WWW] Available: http://products.asminternational.org/hbk/index.jsp. [Accessed: 22-Sep-2011].

[10] Fritz, J.D. Effects of Metallurgical Variables on the Corrosion of Stainless Steels in ASM Handbook Volume 13A Corrosion: Fundamentals, Testing, and Protection (2003), pp. 266-274.

[11] Cunat, P-J. Alloying Elements in Stainless Steel and Other Chromium-Containing Alloys. Euro Inox (2004). [WWW] Available: http://www.euro-inox.org/htm/p_3_EN.html. [Accessed: 13-Sep-2011].

[12] Lindroos, V., Sulonen, M., Veistinen, M. Uudistettu Miekk-ojan Metallioppi. (1986), p. 841.

[13] Poweleit, D. Steel Castings Properties. ASM Handbooks Online (2008). [WWW] Available: http://products.asminternational.org/hbk/index.jsp. [Accessed: 13-Sep-2011].

[14] Davis, J.R. (ed.) Corrosion of Cast Stainless Steels in ASM Specialty Handbook Stainless Steels. 1st ed. ASM International (1994), pp. 229-237.

[15] Lampman, S. Fatigue and Fracture Properties of Stainless Steels. ASM Handbooks Online (2002). [WWW] Available: http://products.asminternational.org/hbk/index.jsp. [Accessed: 09-Sep-2011].

[16] Miller, B.A. Overload Failures. ASM Handbooks Online (2003). [WWW] Available: http://products.asminternational.org/hbk/index.jsp. [Accessed: 05-Oct-2011].

[17] Korroosiokäsikirja. 2nd ed. KP-Media (2004), p. 930.

[18] Vander Voort, G.F. Embrittlement of Steels in Metals Handbook Volume 1. 1st ed. ASM International (1990), pp. 689-736.

[19] Garin, J.L., Mannheim, R.L. Sigma-phase Precipitation upon Industrial-Like Heating of Cast Heat-Resistant Steels. Journal of Materials Processing Technology, vol. 209, no. 1 (2009), pp. 3143-3148.

[20] Hall, E.O., Algie, S.H. The Sigma Phase. International Materials Reviews, vol. 11, no. 1 (1966), pp. 61-88.

[21] Padilha, A.F., Plaut, R.L. Phase Transformation and Microstructure in Duplex Stainless Steels. (2009), pp. 115-140.

[22] Failures Related to Casting. ASM Handbooks Online (2003). [WWW] Available: http://products.asminternational.org/hbk/index.jsp. [Accessed: 05-Oct-2011].

[23] Chandra, T., Kuchlmayr, R. Effect of Strain Rate on Sigma Formation in Ferrite-Austenite Stainless Steel at High Temperatures. Journal of Materials Science, vol. 23 (1988), pp. 723-728.

[24] Garcés, G.R., Coze, J.Le, Garin, J.L., Mannheim, R.L. σ-phase Precipitation in Two Heat-Resistant Steels – Influence of Carbides and Microstructure. Scripta Materialia, vol. 50, no. 5 (2004), pp. 651-654.

[25] Schwind, M., Källqvist, J., Nilsson, J-O, Ågren, J., Andrén, H-O. σ-Phase Precipitation in Stabilized Austenitic Stainless Steels. Acta Materialia, vol. 48 (2000), pp. 2473-2481.

[26] Sims, W.C., Hagel, C.T. The Superalloys. John Wiley & Sons (1972), p.614.

[27] Blachowski, A., Cieślak, J., Dubiel, S.M., Zukrowski, J. Effect of Titanium on the Kinetics of the σ-Phase Formation in a Small Grain Fe-Cr Alloy. Journal of Alloys and Compounds, vol. 308 (2000), pp. 189-192.

[28] Blachowski, A., Cieślak, J., Dubiel, S.M., Zukrowski, J. Effect of Titanium on the Kinetics of the σ-Phase Formation in a Coarse-Grained Fe-Cr Alloy. Intermetallics, vol. 8 (2000), pp. 963-966.

[29] Glossary of Material Testing, Instron. [WWW] Available: http://www.instron.us/wa/glossary/Impact-Strength.aspx#9. [Accessed: 22-Nov-2011].

[30] Rodríguez, J., Haro, S., Velasco, A., Colás, R. A Metallographic Study of Aging in a Cast Heat-Resisting Alloy. Materials Characterization, vol. 45 (2000), pp. 25-32.

[31] Lopez, N., Cid, M., Puiggali, M. Influence of σ-phase on Mechanical Properties and Corrosion Resistance of Duplex Stainless Steels. Corrosion Science, vol. 41 (1999), pp. 1615-1631.

[32] Davis, J.R. (ed.) ASM Specialty Handbook Stainless Steels. 1st ed. (1994), p. 577.

[33] SFS-EN ISO Standard 148-1 Metallic Materials. Charpy Pendulum Impact Test. Part 1: Test Method. (2009).

[34] Sahin, M., Akata, H.E. An Experimental Study on Friction Welding of Medium Carbon and Austenitic Stainless Steel Components. Industrial Lubrication and Tribology, vol. 56, no. 2 (2004), pp. 122-129.

[35] Charpy Impact Test. Engineering 2 Production Inc. [WWW] Available: http://www.e2pro.us/home/images/charpy.png. [Accessed: 16-Jan-2012].

[36] Vander Voort, G.F. Metallography Principles and Practice. ASM International (1999), p. 752.

[37] Babakr, A.M., Al-Ahmari, A., Al-Jumayiah, K., Habiby, F. Sigma-Phase Formation and Embrittlement of Cast Iron-Chromium-Nickel (Fe-Cr-Ni) Alloys. Journal of Minerals & Materials Characterization & Engineering, vol. 7, no. 2 (2008), pp. 127-145.